JOURNAL OF SPACECRAFT AND ROCKETS
Vol. 43, No. 6, November–December 2006

Laminar-Turbulent Transition on Reentry Capsules and Planetary Probes

Steven P. Schneider*
Purdue University, West Lafayette, Indiana 47907-1282

DOI: 10.2514/1.22594

Introduction

NASA interest in reentry vehicles has recently taken a dramatic shift away from lifting bodies (X-33, X-38) and winged vehicles (shuttle, X-34) towards capsules. This follows the loss of the *Columbia* and the Presidential announcement of a program focused on the moon and Mars [1]. The Presidential Commission report mentions "entry, descent, and landing: precision targeting and landing on 'high-*g*' and 'low-*g*' planetary bodies" as one of 17 critical areas identified for the initial focus ([1], p. 28).

NASA is developing a crew exploration vehicle (CEV) to fulfill these missions, following the planned retirement of the shuttle circa 2010. It has been determined that this CEV is to be an Apollo-like capsule. Although moderate levels of lift can much improve the safety and flexibility of entry trajectories ([2], Chap. 6), the Apollo geometry is proven in the very high aeroheating of a moon-return entry {11 km/s ([3], p. 19)}, and easier to integrate with a launch-escape rocket. The same CEV reentry geometry is to be used for both the low-energy entries from low earth orbit (LEO) and the very different high-energy entries from hyperbolic lunar and interplanetary missions. The planetary program also continues to fly blunt bodies as entry probes; it seems efficient to consider these similar shapes in parallel with the capsules.

Transition is one aerothermodynamic problem that is not yet well understood. Will the uncertainties in estimating transition [4] impact the design of these vehicles? Is transition important to the development of new capsules a la Mercury, Gemini, Apollo, or Soyuz? It is generally thought that transition is more important for slender vehicles than for blunt vehicles, although few studies have been carried out to support this idea [5]. Because there is much uncertainty about the properties of any such capsules (geometry, ballistic coefficient, mission needs, and so on), this question cannot be answered definitively. Nevertheless, the following reviews the public-domain literature from blunt-body and capsule programs, with a view towards identifying the available data for transition under these conditions, the physics of the transition process, and the conditions where laminar-turbulent transition is important. Particular attention is paid to manned capsules, where funding levels are likely to support more detailed analyses. Although the Russian Soyuz vehicle may be an important forerunner to the CEV [6], detailed technical information was not available to the author, so it is not discussed. This survey, updated from [7], is certainly incomplete, and the author would appreciate any additional information that the reader might be able to provide.

Laminar-turbulent transition in hypersonic boundary layers is important for prediction and control of heat transfer, skin friction, and other boundary layer properties. Vehicles that spend extended periods at hypersonic speeds may be critically affected by the uncertainties in transition prediction, depending on their trajectories, geometries, and surface properties. However, the mechanisms leading to transition are still poorly understood, even in low-noise environments.

Many transition experiments have been carried out in conventional ground-testing facilities over the past 50 years [4]. However, these experiments are contaminated by the high levels of noise that radiate from the turbulent boundary layers normally present on the wind tunnel walls [8]. These noise levels, typically 0.5–1% of the mean, are an order of magnitude larger than those observed in flight [9,10]. These high noise levels can cause transition to occur an order of magnitude earlier than in flight [8,10]. In addition, the mechanisms of transition operational in small-disturbance environments can be changed or bypassed altogether in high-noise environments; these changes in the mechanisms change the parametric trends in transition [9]. Although transition can become completely dominated by roughness [11] or perhaps ablation effects, these effects are usually only one of several factors whose effect must be understood to reliably predict flight [9,12]. Because no single ground-test facility can simultaneously duplicate the velocity, scale, freestream noise, freestream chemistry, and surface temperature of reentry flight, partial simulations in the available facilities must be combined to develop computational models that can then be extrapolated to flight.

Mechanism-based methods must be developed to provide reliable predictions. Such mechanism-based prediction methods are now becoming feasible for complex three-dimensional flows at hypervelocities, due to ever-increasing computational capabilities. For example, Johnson et al. recently provided stability-based transition analyses for a planetary probe, although their preliminary results are only for a simplified axisymmetric case [13]. Because the best mechanism-based methods will still require many assumptions, development and validation will require measurements of the

Steve Schneider received his B.S. from the California Institute of Technology in 1981. From 1981 to 1983, he worked at the Naval Ocean Systems Center in San Diego. Steve returned to Caltech in 1983, receiving an M.S. in 1984 and a Ph.D. in aeronautics in 1989. His thesis involved experimental measurements of low-speed laminar instability and transition. He joined Purdue as an Assistant Professor in July 1989. Since then, he has focused on high-speed boundary-layer transition, developing facilities and instrumentation for detailed measurements under quiet-flow conditions. A $1 million 9.5-inch Mach-6 quiet-flow Ludwieg tube was completed in 2001, and achieved high Reynolds number quiet flow in 2006. He was promoted to Professor in 2004, and has written five review articles on hypersonic transition.

Presented as Paper 4763 at the 35th Fluid Dynamics Conference, Toronto, 6–9 June 2005; received 23 January 2006; revision received 18 April 2006; accepted for publication 1 June 2006.

*Professor, School of Aeronautics and Astronautics. Associate Fellow AIAA.

mechanisms in ground-test facilities, and calibration of the transition estimates using flight data. Although most of the existing data for transition on capsules and planetary probes were obtained when computational capabilities were very limited, the experimental data from ground test and flight were expensive to obtain, and remain useful.

General Issues for Blunt-Faced Capsules

Horvath et al. reviewed the effects of transition on NASA reentry vehicles, focusing on measurements in the hypersonic tunnels at Langley [14]. Figure 1 outlines the features of the blunt-body flowfields. The payload volume aft of the heat shield is limited by the need to avoid high levels of heating that may appear if the separated shear layer reattaches. Horvath et al. also review transition on other vehicles such as the X-33, X-38, X-43, and space shuttle.

Wright et al. review aeroheating issues for the afterbodies of planetary probes [15,16]. Wright discusses the importance of transition to the prediction of afterbody heating, and cites references that suggest that transition occurred on the afterbodies of a Viking Lander and on the European ARD test vehicle.

Example: Two Mars Probes

Edquist et al. provide an excellent discussion of the general issues for aeroheating on capsule faces, in the context of a planetary-probe program, the Mars Smart Lander (now the Mars Science Laboratory) [17,18]. The paper presents cold-flow experiments and Navier–Stokes computations using two different codes.

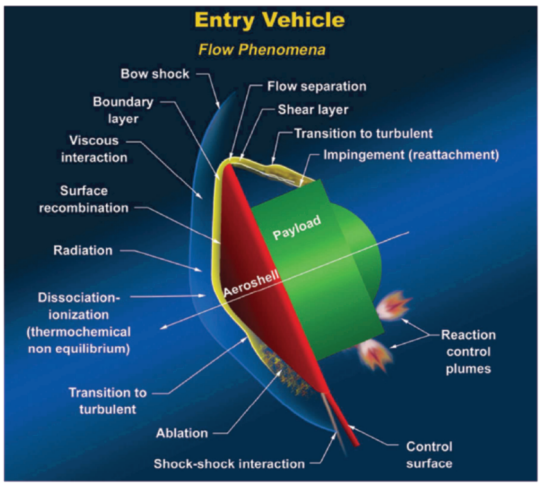

Fig. 1 Hypersonic blunt-body flow. From [14].

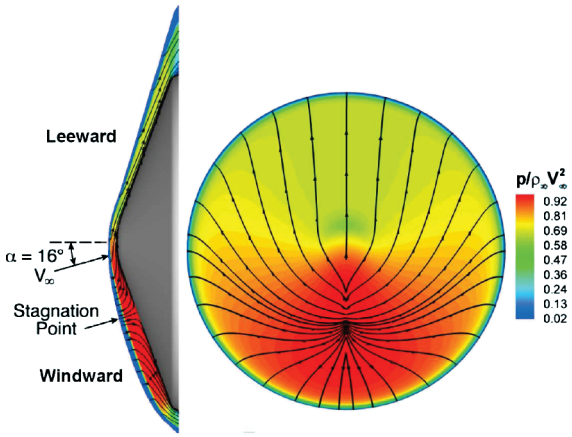

Fig. 2 Mars Smart Lander: LAURA solutions for symmetry plane and surface pressure and streamlines at nominal peak heating from [17].

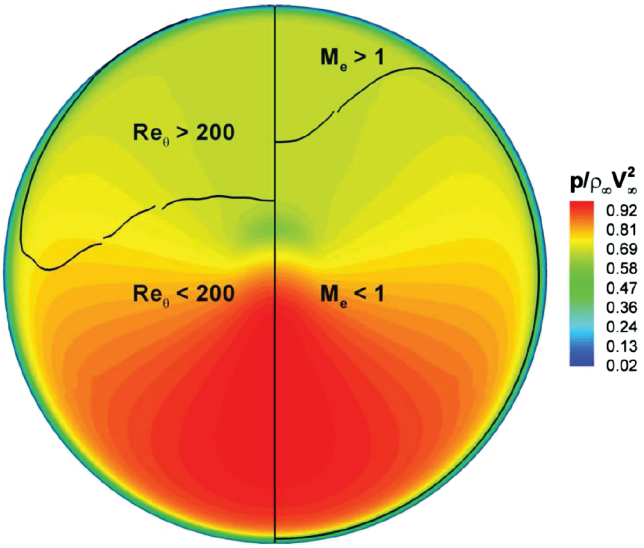

Fig. 3 Mars Smart Lander: LAURA solutions for surface pressure, $Re_\theta = 200$, and $M_e = 1$ at nominal peak heating from [17].

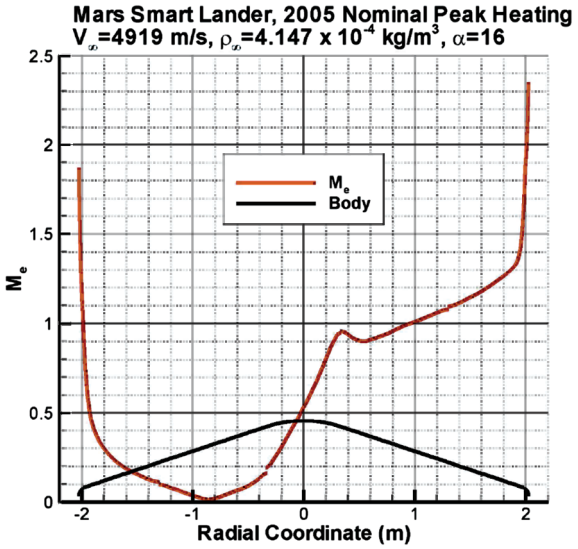

Fig. 4 Mars Smart Lander: LAURA solution for edge Mach number at nominal peak heating.

Figures 2 and 3 show the streamlines and the momentum-thickness Reynolds number, Re_θ, for the 70-deg half-angle blunted cone at an angle of attack (AOA) of $\alpha = 16$ deg. The stagnation point is towards the windward side; flow travels pseudoradially from here towards the rim, providing a longer boundary-layer fetch towards the lee side. The Mach number at the boundary-layer edge, M_e, is below 1 over most of the face, despite the high freestream velocity, due to the blunt shape. The peak edge Mach number is only 1.3 at the lee rim, as shown in Fig. 4 (provided by Karl Edquist, private communication, August 2004). Strictly speaking, these boundary layers are thus subsonic and only slightly supersonic, because the edge Mach numbers are not hypersonic.

At the peak heating condition, Re_θ is below 200 on the windward side and above 200 for most of the lee face; 200 was taken as an estimate for transition onset. Assuming turbulent flow, the peak heating would be 70% higher than if laminar, whereas an all-turbulent flow would have 38% higher total heat load than an all-laminar flow. This paper shows that transition can be a significant issue for the heating to the blunt face, and that transition is more likely on the lee side of the blunt face at AOA.

Horvath et al. provide an equally good discussion of aeroheating to the afterbodies [19,20]. A shear layer separates from the edge of the

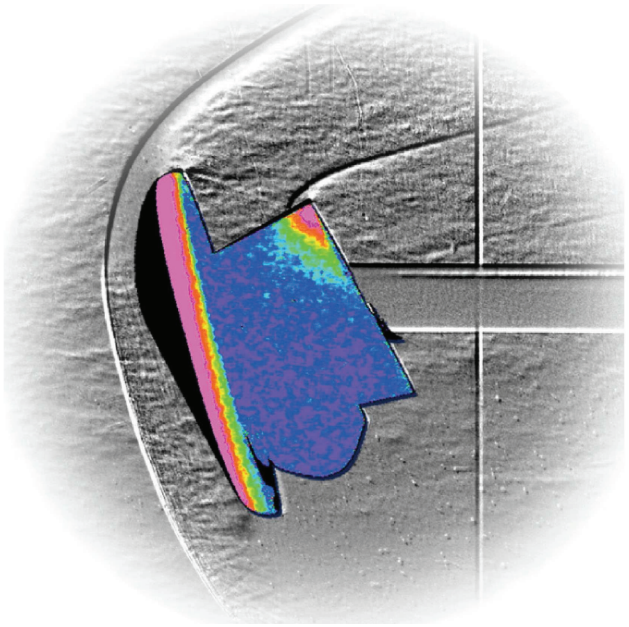

Fig. 5 Shear layer reattachment on Mars Sample Return Orbiter. From Fig. 6 in [14] and cover of [19].

blunt face, but can reattach to the afterbody depending on geometry. Figure 5 shows experimental data from the Mars Sample Return Orbiter, as an example; this figure combines a schlieren image with a surface heat-transfer image to show the bow shock, shear layer separation and reattachment, and the resulting localized peak heating on the afterbody. The data were obtained in the Mach-6 tunnel at NASA Langley under unknown conditions. At a reattachment, the localized heating could reach a maximum of 40–75% of the stagnation-point heating, a very high value. Shear layer turning angles of 30–40 deg were measured. Transition either in the shear layer or upstream of the separation point has a big effect on both the turning angle and the reattachment heating. A wake correlation was used to estimate transition in the shear layer.

Design Issues

Smith lays out the general design issues for blunt reentry vehicles like capsules and planetary probes [21]. Most of the planetary probes are designed on very limited budgets, leading program managers to choose heritage technology to limit cost and risk. Smith also clarifies that simple inviscid-boundary-layer methods are used for most of the designs, with transition estimated based on an Re_θ criterion, with 140 considered conservative ([21], p. 4-15). Smith believes that the available transition database for blunt vehicles is small, which is a concern because "transition uncertainty prior or close to peak heat flux significantly affects the TPS sizing." Pages 4-12 and 4-15 in Smith also make clear that reattachment of the separated shear layer is to be avoided because it can cause problems with locally high reattachment heating and aerodynamic instabilities. Smith apparently uses simple correlations and then Navier–Stokes codes to estimate reattachment, although details are not given. Smith believes that because the boundary-layer on the base of the Huygens probe is thin, the laminar or turbulent state has little effect (pp. 4–15); however, he seems to miss considering the effect of transition on the separation of the shear layer.

Summary of Issues

These papers describe the two major ways in which transition appears to be relevant for blunt capsules and planetary probes. The first is transition on the blunt face, which can have a significant effect on heating, depending on ballistic coefficient, angle of attack, geometry, roughness, and so on. The second is the effect of transition on the shear layer that separates from the rim of the blunt face. This shear layer may be important, if it may reattach to the afterbody, or otherwise affect the aerodynamic stability or the aerothermodynamic heating. Sinha et al. [22] show that transition in the wake can have a significant effect on base heating. Transition may or may not occur in the shear layer in a significant way, again depending on the configuration and trajectory.

For the designer, one issue is whether transition has a significant effect on the thermal protection system mass via increased heating. The other issue is the effect on lift-to-drag ratio through changes in the afterbody flow that affect moments and the trim angle of attack.

Mercury

Sommer et al. measured the static and dynamic stability of Mercury capsules in the ballistic range at NASA Ames [23]. A typical shadowgraph is shown in Fig. 6, where the yaw angle is 0.9 deg and the Reynolds number based on freestream conditions and diameter $Re_D = 2.50 \times 10^6$. At low angles of attack the flow is separated over the entire afterbody; note that nominal reentries were flown near zero angle of attack. The boundary layer on the front face was believed to be laminar, although this could not be demonstrated directly; this laminar boundary layer separates around the corner, transitions to turbulence, and remains separated.

"To determine whether a turbulent boundary layer on the model front face would induce flow attachment on the afterbody, a model with the front face roughened to promote turbulence was tested." Fig. 7 shows the attached afterbody flow that resulted, at a yaw angle of 0.9 deg and $Re_D = 2.44 \times 10^6$. The change in the flow pattern is dramatic. When the flow reattaches on the conical section, a compression shock forms at the beginning of the cylindrical section, which will lead to high heating rates there, as shown in Figs. 10 and 11. Unfortunately, the roughness required to achieve front-face turbulence was not studied; only Fig. 8 is shown to document the roughness used. Figure 9 shows that similar reattachment occurred with a smooth front face in another test at $M_\infty = 5.3$ and a high $Re_D = 3.3 \times 10^6$, again suggesting an effect of transition on the front face ([23], p. 9).

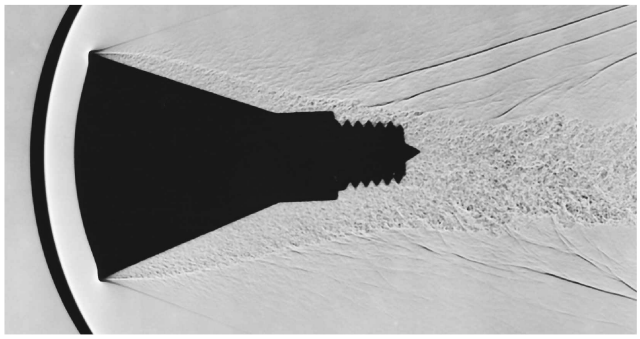

Fig. 6 Separated flow on smooth-faced Mercury capsule at Mach 3.28 and 2.0 deg AOA. From Fig. 11a in [23].

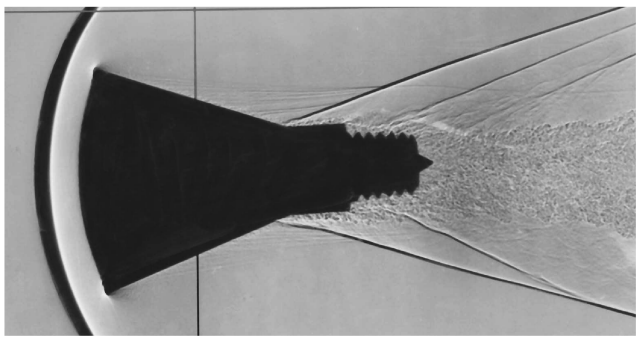

Fig. 7 Attached flow on rough-faced Mercury capsule at Mach 3.28 and 2.4 deg AOA. From Fig. 11b in [23].

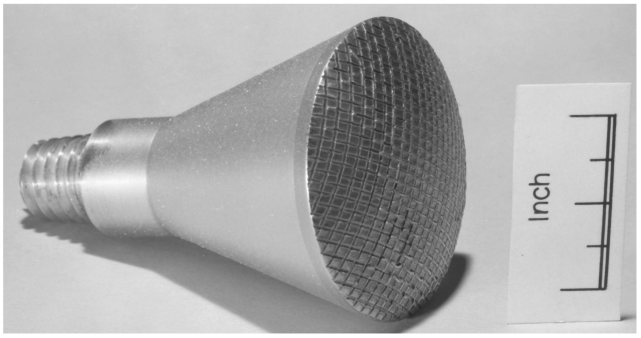

Fig. 8 Photograph of Mercury capsule model with rough front face. From Fig. 10 in [23].

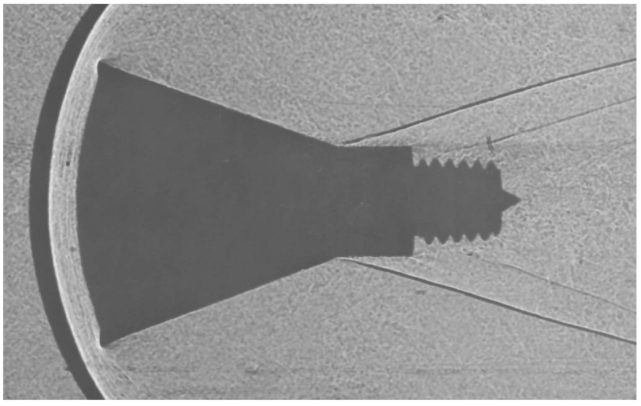

Fig. 9 Attached flow on smooth-faced Mercury capsule at Mach 5.34 and 0.5 deg AOA. From Fig. 9 in [23].

Although the configuration was statically stable, it was dynamically unstable, with a dynamic-stability parameter ranging from 1 to 6 when the afterbody flow was separated. When the roughened face produced an attached afterbody flow, the dynamic instability increased, with the parameter increasing to 14.4. Transition had a marked effect on dynamic instability; presumably the same physics would also have a marked effect on aeroheating.

Taylor et al. measured pressure and heat-transfer distributions on the Mercury capsules in the Unitary Plan tunnel at NASA Langley [24]. The flow separates at the junction of the blunt face and the conical afterbody, as can be seen in Fig. 10, particularly on the windward (lower) side. This results in low heat transfer on the conical cabin section, as shown in Fig. 11. Here, the horizontal axis is the arc

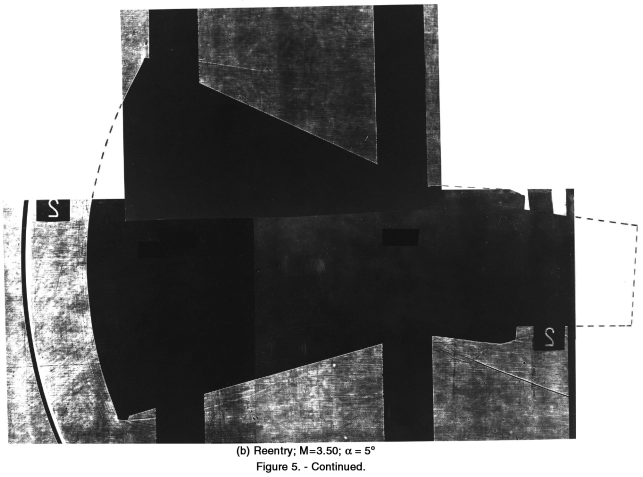

Fig. 10 Shadowgraph of Mercury capsule at $\alpha = 5$ deg and Mach 3.50. Enhanced from Fig. 5b in [24].

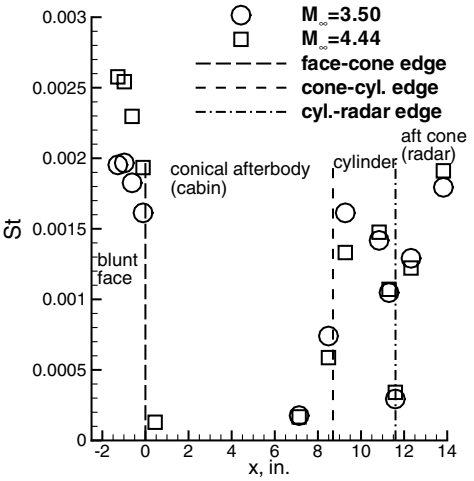

Fig. 11 Stanton number distribution on Mercury capsule at zero AOA. From Fig. 9a and Table 5 in [24].

length from the edge of the blunt face, and the vertical axis is the Stanton number. However, the separated flow reattaches; in Fig. 10 on the windward conical section this occurs about 2/3 of the way to the junction with the cylindrical parachute canister. The compression corner at the canister generates a compression shock and heat-transfer coefficients that are 85% of the stagnation heating at Mach 3.50 and 60% at Mach 4.44. The locations of transition and reattachment are uncertain. The vertical bars in the photo are part of the window support frame. The Reynolds number based on freestream conditions and capsule diameter was 2.5×10^6 for the Mach 3.5 measurements and 2.7×10^6 for the Mach 4.4 measurements, and transition was allowed to occur naturally. Curiously, weak waves are just visible in front of the blunt face in Fig. 10, parallel to the face.

Everhart and Bernot clarify the flowfield concept by providing oil-flow and schlieren images at Mach 6.9 and 9.6 in the Langley 11-inch tunnel [25]. Figure 12 shows an oil-flow of a 2.25-in.-diam model at $Re_D = 0.24 \times 10^6$, where the oil is painted on in a continuous film. The flow separates just aft of the junction between the blunt face and the conical afterbody, and reattaches about 2/3 of the way down the cylindrical section. Prerun brush strokes are evident in the oil in the separated region on the conical afterbody. Figure 13 shows the flow of oil under the same conditions, except that the oil is applied in small

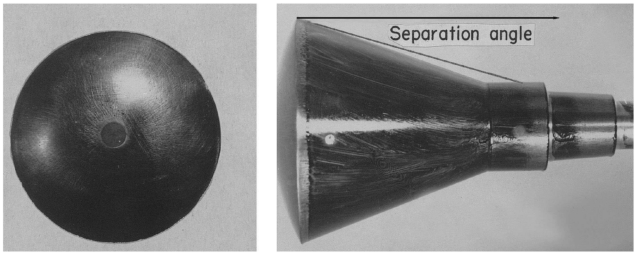

Fig. 12 Oil-flow study of sting-mounted Mercury model at zero AOA and Mach 6.9. From Fig. 7a in [25].

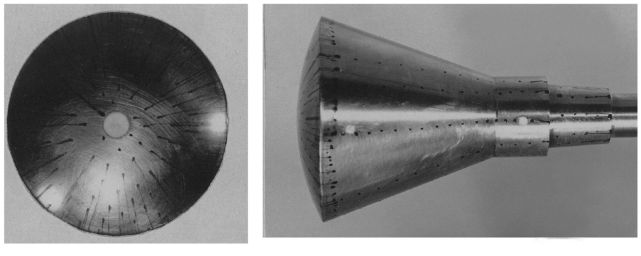

Fig. 13 Oil-flow study of sting-mounted Mercury model at zero AOA and Mach 6.9. From Fig. 7b in [25].

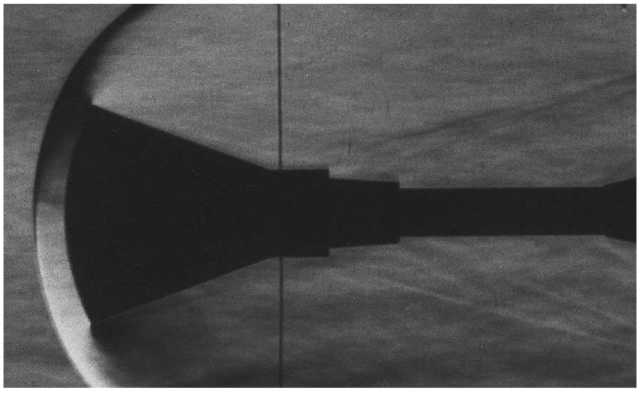

Fig. 14 Schlieren of sting-mounted Mercury model at zero AOA and Mach 6.9. From Fig. 5a in [25].

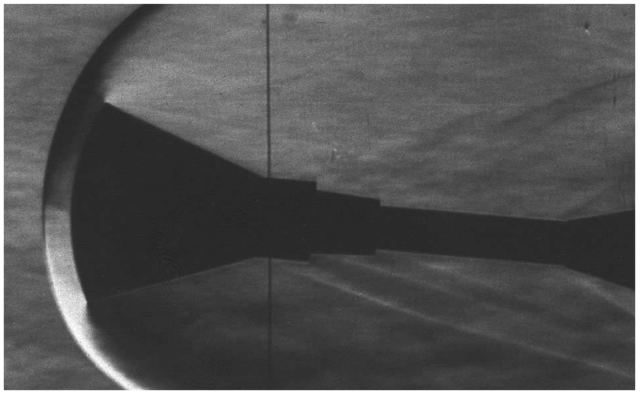

Fig. 15 Schlieren of sting-mounted Mercury model at 5 deg AOA and Mach 6.9. Enhanced from Fig. 5b in [25].

dots. The dots form streaks only in the attached-flow regions where the shear is significant; they again show separation just aft of the face–cone junction, with reattachment roughly 2/3 of the way along the cylinder. There is an additional separation and reattachment downstream of the cylindrical portion. Figure 14 shows the corresponding schlieren image; the separation is barely visible on the lower surface in this low-density flow. Figures 15 and 16 show the corresponding schlieren and oil-flow images at 5 deg AOA, near the typical range of the flight vehicle. Figure 15 shows a compression shock at the beginning of windward side of the cylindrical section that is noticeably more visible than for the zero AOA case. Figure 16 shows the windward flow does not quite reattach even at the end of the cylinder section; it also shows the crossflow on the cylinder section from wind to lee.

Reller and Seegmiller reviewed pressure and heat-transfer measurements from the Mercury program [26]. Whereas the heating on the conical afterbody section was in reasonable agreement with simple laminar or transitional boundary-layer theory, the heating on the cylinder was near a simple turbulent theory when at zero AOA, and well above simple theories when at AOA ([26], Fig. 19). Because the theories all predicted heating to decrease with arc length whether laminar or turbulent, heating that showed an increase with arc length was interpreted to be transitional. The heating to the windward ray of the cylindrical section was more than twice the leeward heating, when at an AOA of only 2 deg; this sudden shift was thought to be due to transition ([26], Fig. 21). Heating rates of as much as 90% of stagnation were measured on the cylindrical portion; these could be explained by assuming a turbulent boundary layer originating at the cone–cylinder junction, which resulted in a local heating rate that was 85% of the stagnation value ([26], p. 26). Reller and Seegmiller conclude:

> Boundary-layer separation is the most important single factor affecting afterbody pressures and heat-transfer rates. It is related to the existence of a laminar boundary-layer condition at the edge of the heat shield and a laminar free-boundary condition on the afterbody. When separation occurs, it is often followed by transition to turbulent flow within the free boundary at relatively low Reynolds numbers and a subsequent flow reattachment. This situation is characteristic of the test configuration and gives rise to very substantial afterbody heating rates.

Reller and Seegmiller isolated one factor in this separating and transitioning flow, as shown in Fig. 17. The heat-transfer coefficient is plotted against the arc length along the afterbody surface from the edge of the blunt face, normalized by the radius of the body. To determine the effect of model temperature, Reller and Seegmiller fabricated a model with a solid copper heat shield to provide a cold wall (the open symbols), instead of the usual thin steel shell that provides a near-adiabatic wall (the solid symbols). The measure-

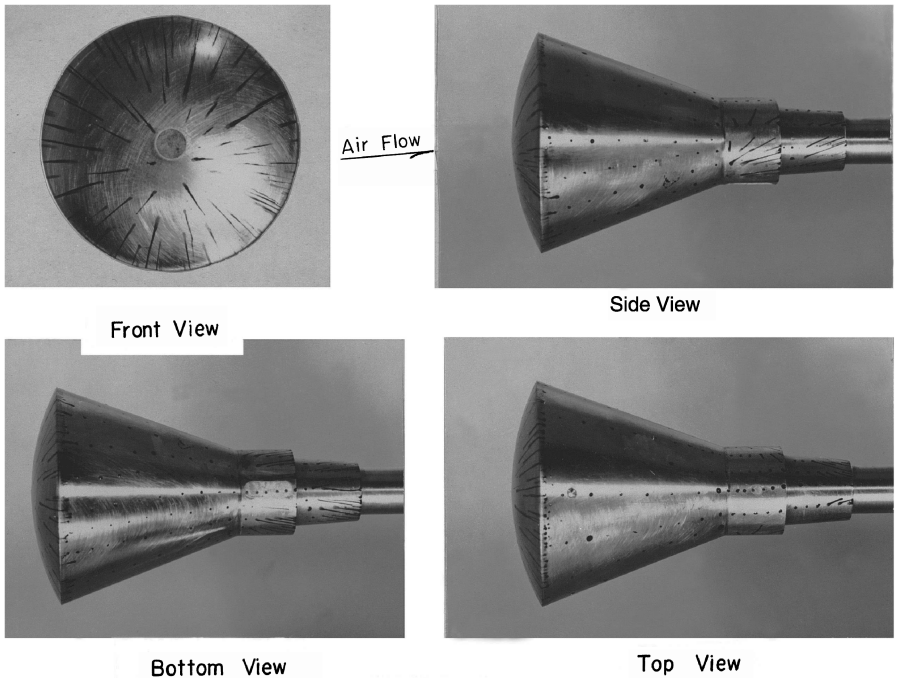

Fig. 16 Oil-flow study of sting-mounted Mercury model at 5 deg AOA and Mach 6.9. From Fig. 7c in [25].

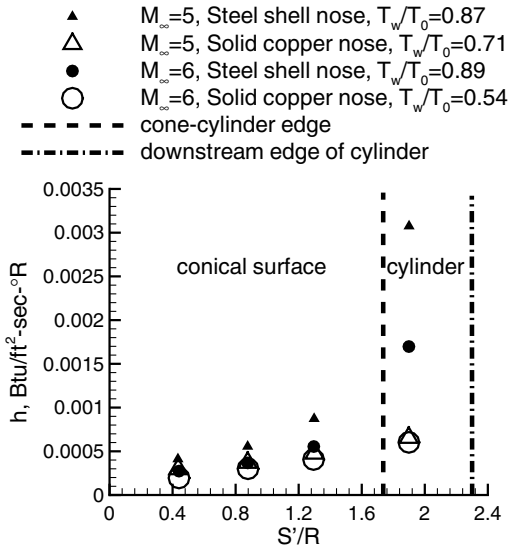

Fig. 17 Effect of heat-shield temperature on afterbody heating to Mercury capsule at zero AOA. From Fig. 20 in [26].

ments were made in the NASA Ames 10 × 14-in. supersonic wind tunnel, using models precooled by injecting liquid nitrogen into the tunnel throat. The wall temperature, T_w, divided by the tunnel stagnation temperature, T_0, is shown for each case. The Reynolds number based on body diameter and freestream conditions was $Re_D = 5.87 \times 10^5$ at a freestream $M_\infty = 5.03$ and $Re_D = 2.86 \times 10^5$ at $M_\infty = 5.96$, on 2-in.-diam models.

The copper model had a much lower surface temperature, but conditions (including tunnel noise) were otherwise the same. The heat-transfer coefficients are lower with a cold wall, and much lower on the cylindrical section. This suggests that the cold wall maintains a laminar boundary layer on the cylindrical section (as might be expected at these low edge Mach numbers [4]) and thus a heating rate that is three to five times lower. It would be interesting to compare to a modern computation.

Erb and Jacobs discuss the reentry performance of the Mercury heat shield [27]. The first two flights by Shepard and Grissom used a beryllium heat-sink heat shield. This was later replaced with an ablator to reduce cost and weight. The spherical-segment face reentered at 4 deg AOA; note that the blunt face that reenters forward is called the "aft" face in much of the Mercury literature. The afterbody cone had a 20-deg half-angle; this combined with the small AOA apparently avoided the shear-layer impingment issues described in [17]. The heating on the blunt face appeared to be uniform. The afterbody heat shield is only mentioned in a single sentence.

O'Neal and Rabb analyzed flight data for heating to the blunt face of the Big Joe flight test of the Mercury spacecraft [28]. At 370 kft. the flight-path angle was about −4 deg and the velocity was about 21 kft/s. The heating rates were below design levels due to booster-separation problems. The vehicle ran out of control-thruster fuel due to these same booster-separation problems, and reentered at angles of attack that oscillated in a 20-deg range centered near 6 deg. The heating levels were fairly uniform over the whole blunt face, and compared well with laminar theory, indicating that the forebody flow remained laminar. It was thought that this was due to a low Reynolds number, which did not exceed $Re_x = 0.5 \times 10^6$ until approximately 590 s into the flight, at 105 kft when the velocity was about 11 kft/s ([28], p. 13). Here, Re_x is the usual Reynolds number based on edge conditions and arc length from the stagnation point.

Stephens analyzes flight data for afterbody heating to the same Big Joe flight test of the Mercury spacecraft [29]. Heating was fairly nominal except on the cylindrical afterbody, where the skin buckled and two recovery hooks were badly burned, as shown in Figs. 18 and 19. It appears that the separated shear layer reattached turbulent onto the cylindrical section. Both theory and wind tunnel failed to predict these high heating rates.

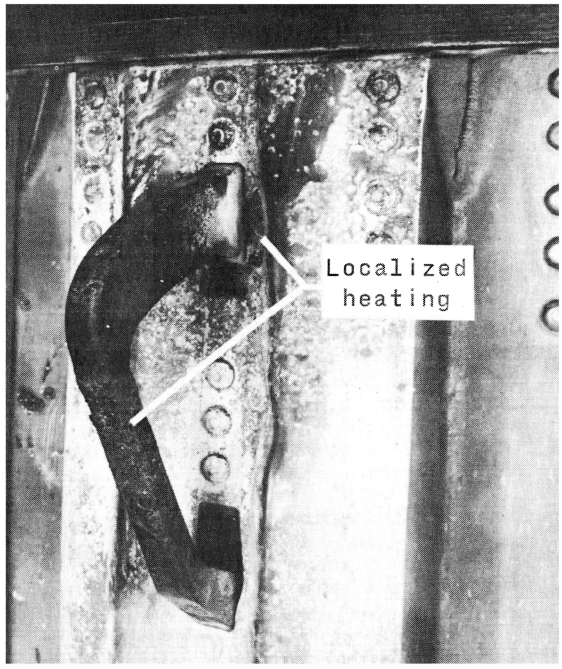

Fig. 18 Results of localized heating on Mercury spacecraft: hook located in pitch plane. From [29].

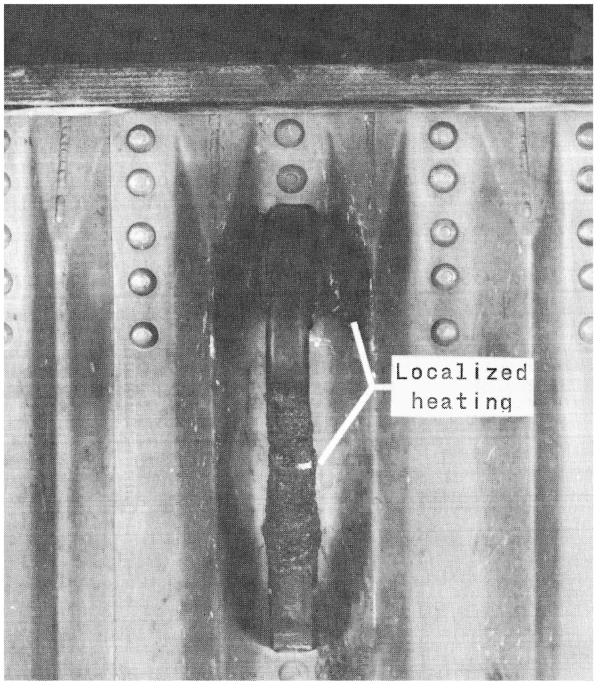

Fig. 19 Results of localized heating on Mercury spacecraft: hook located in quadrant 2. From [29].

Weston and Swanson analyze ground and flight data for heating to the Mercury afterbody [30]. The heating to the cylindrical afterbody is turbulent for Reynolds numbers based on heat-shield diameter of 0.5 million or more, and laminar for Reynolds numbers of 0.2 million or less. The Big Joe flight data appeared consistent with the wind-tunnel results. Heating rates on the cylindrical afterbody approached 80% of laminar stagnation-point values.

Murphy also analyzed four Mercury flights to assess afterbody heating [31]. Flights MA-5, MA-7, and MA-8 flew with small trim angles, but flight MA-2 reentered with a large trim angle of about 12.5 deg. The forward end of the conical section exhibits an unexplained rise in heating at about 220 s for all three nominal flights.

On the aft end of the conical section and on the cylinder, the heating rates overshoot above turbulent levels and then recover to those predicted by simple turbulent theories. This gave a strong indication of transition onset on the conical part of the body for Reynolds numbers of $Re_x \simeq 200,000$–$500,000$, where Re_x is based on arc length from the stagnation point and conditions at the boundary-layer edge. For flight MA-2 at angle of attack, transition also seems to have occurred, but the vehicle was rolling and the slow instrumentation could only capture the roll-averaged effect. The three near-repeated flights near zero angle of attack seem worthy of a reanalysis with modern techniques.

Gemini

Introduction

Figure 20 shows a schematic of the Gemini reentry capsule. The blunt face is a section of a sphere, and is followed by a conical section with a 20-deg half-angle, a cylindrical section containing reaction control system (RCS) jets, and the conical rendezvous and recovery (R&R) section.

Figure 21 shows that the geometry was scaled up from the Mercury capsule with few changes. Separation and attachment on the afterbody has a big effect on aerodynamic stability; Gemini was more stable than Mercury at Mach 3, due to reattachment at the aft end at low angles of attack, but the two configurations had similar stability at Mach 9.5 when the reattachment was similar [32].

Gemini Aerodynamics and Trajectories

Mitchell et al. [33] review Gemini operations, and mention landing accuracy. Figure 22 shows that initial flights missed the preflight prediction by as much as 90 nm, whereas later flights scattered within about 5 nm; a CEP (circular error probable) is not given. It appears that the aerodynamics learned from the earlier flights were used to correct the guidance software for later flights.

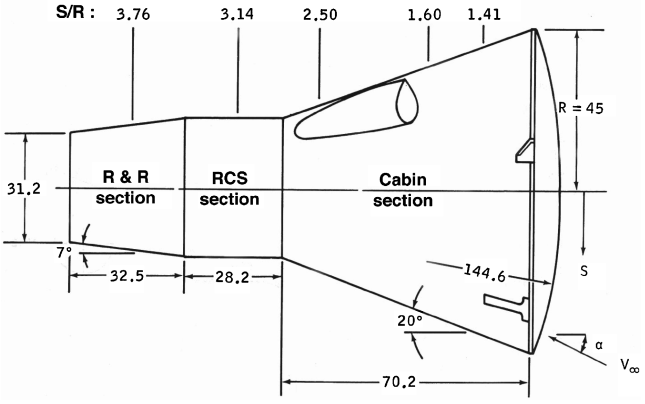

Fig. 20 Schematic of Gemini capsule. From [15,44]. Dimensions in inches.

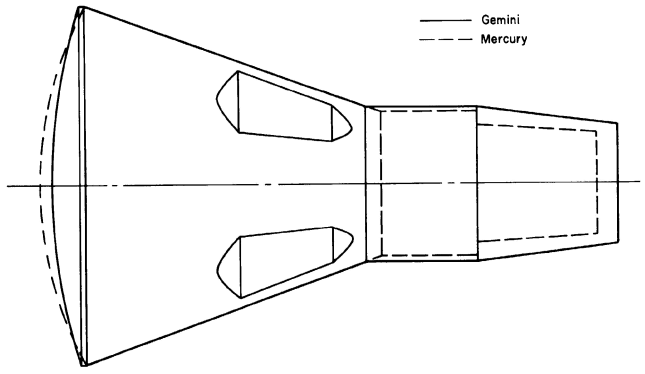

Fig. 21 Schematic comparing Gemini and Mercury geometries. From Fig. 1 in [32].

Box et al. [34] provide additional information regarding the reentry accuracy and associated guidance. An overview is provided for the two forms of guidance logic that were used, and detailed descriptions are provided for each flight, including the accuracy and the sources of error. The constant bank-angle guidance logic was ineffective for missions of long duration where a large center-of-gravity movement caused a significant shift in trim AOA and aerodynamics, or when the aerodynamics were uncertain for other reasons, such as in the initial flights. However, the rolling-reentry guidance technique was able to adapt to uncertainties in the aerodynamics, and provide an accurate reentry (within a few miles) regardless, as long as the target point was within the feasible footprint. For future developments, these two papers show that it is a question of whether it is worth reducing risk by low-cost ground-based research and development before determining the expensive flight-derived aerodynamics. It appears that appropriate guidance logic can correct for most errors, so the preflight determination of lift-to-drag ratio (L/D) can retain significant uncertainties.

Griffith reviews the trim AOA and L/D ratio for the Gemini flights, and compares the flight data to the wind tunnel [35]. Preflight predictions of these quantities were significantly in error at higher Mach numbers early in the reentry. Arnold Engineering Development Center (AEDC) cold-flow wind tunnel measurements at higher Mach numbers and similar values of Re_{2d} do a good job of correlating flight and tunnel data. Here, Re_{2d} is the Reynolds number based on capsule diameter and conditions behind the normal shock. Figure 8 in the reference shows that the center of pressure suddenly shifts by about half the base diameter as Re_{2d} increases from 2400 to 5400. It was thought that this was due to reattachment of the flow around the corner of the heat shield at higher Reynolds number. Griffith's Fig. 9 shows that this center-of-pressure shift corresponds to a trim AOA shift of about 5 deg; the trimmed AOA in flight varied from about 5 to 15 deg below 200 kft. It is not clear whether this shift is reflected in the flight data. This effect appears to be important for design, but may not involve transition, because the Reynolds number is very low. Griffith also shows that a trim-angle error of about 2 deg (uniform over the trajectory) corresponds to a downrange error of about 30 miles ([35], Fig. 15).

Pershing provides a comprehensive review of the ground and flight data, in preparation for a follow-on program that was later canceled. He believes that the trim-angle errors are probably due to high-enthalpy effects [36], noting also that all the ground-test data suffer from low values of the Reynolds number based on diameter and conditions behind the bow shock.

Gemini Aeroheating

Bertin and Cummings mention that shock-interaction heating caused a significant problem for the thermal protection system (TPS) on the afterbody of the Gemini capsules [37], but give no details nor any references. Malik and Souris give a brief description of this problem, which led to burn-through on two 0.016-in. Rene 41 shingles on the afterbody near the umbilical adaptor interconnect fairing, on Gemini II ([38], pp. 16 and 37). Figure 23 appears to be the best image of the surface damage on the windward afterbody. Two small holes were formed, but the underlying insulation was not damaged; more detail is shown in Fig. 24. To correct the problem, the shingles were thickened to 0.025 in. and the AOA was reduced by moving the center of gravity by about 1 in. Malik and Souris do not explain the cause of the problem with the TPS. Collins et al. show a single image, and comment that the high heating only occurred in the wake of a fairing; because wind-tunnel tests of minor changes in the fairing did not reduce the heat intensity, the trim angle was reduced a bit and the shingle thickness was increased ([39], p. 20). More details are given in [40], including five images of the damage. Sheldon [41] describes wind-tunnel tests of the fairing-interaction heating but does not include the results. Technical reports of the McDonnell Company [42,43] tabulate 700 pages of shock-tunnel measurements of the surface heating and pressure in the interaction region, but do not plot or analyze the results.

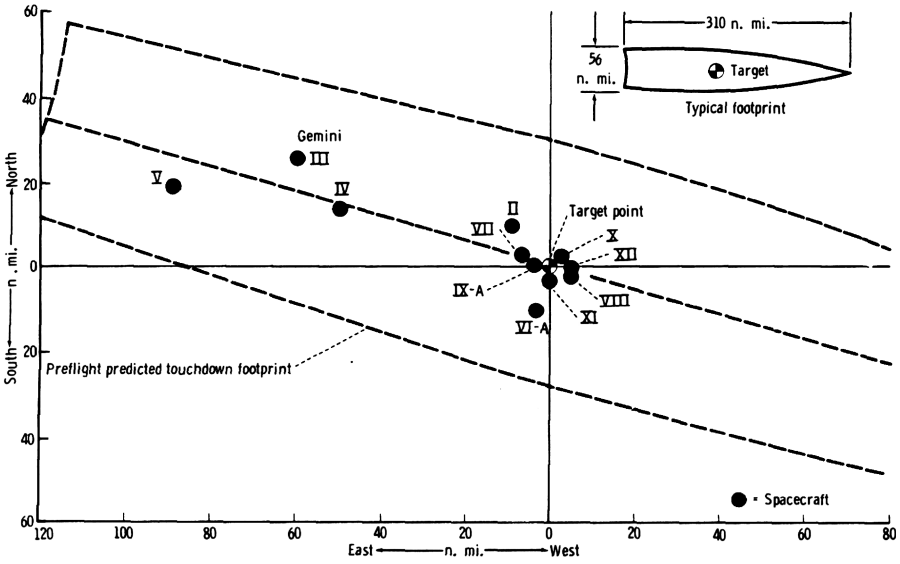

Fig. 22 Landing accuracy for Gemini flights. From Fig. 22-3 in [33].

NASA-S-65-1704

Fig. 23 Effects of reentry heating on the Gemini II spacecraft. From [40] (or [39]).

NASA-S-65-1597

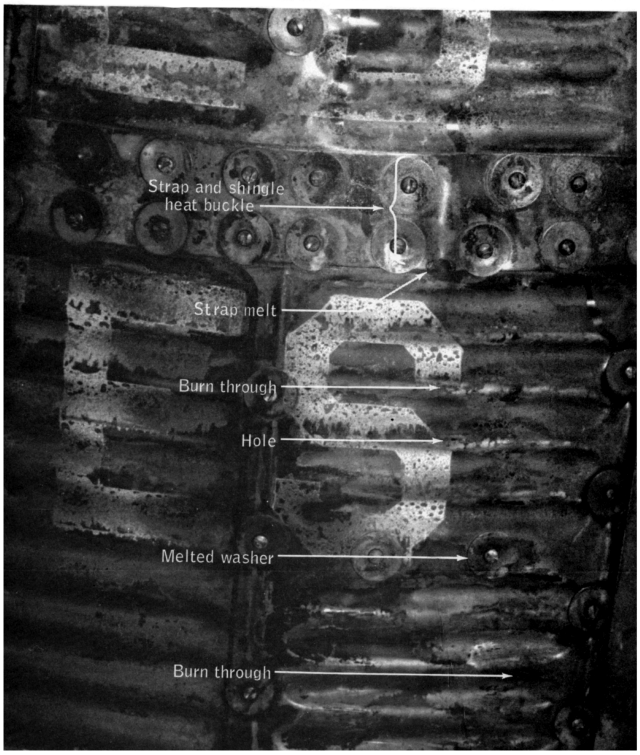

Fig. 24 Closeup of reentry heating damage on the Gemini II spacecraft. From [40].

Raper reviewed wind-tunnel data for pressure, heating, and transition to the afterbody of the Gemini vehicles [44]. Wind-tunnel measurements showed that the peak heating to the afterbody was about 50% of the stagnation-point value on the windward side, and about 28% on the leeward side. The windward side heating is shown in Fig. 25; the vertical axis is the heat-transfer rate normalized with the stagnation-point value at zero angle of attack, whereas the horizontal axis is the arc length from the geometric center of the blunt face, normalized with the maximum body radius. The heating level is low over the conical cabin. It rises markedly over the cylindrical RCS section, to 20–50% of the stagnation-point heating, and then falls to more moderate values over the boattailed R&R section. Clearly, the heating to the RCS section is a real TPS issue. At 40 deg AOA, the windward afterbody heating rose as high as 3.2 times the stagnation-point value, making flight at high attitudes unfeasible [45].

Price et al. obtained similar data at Mach 3.51 and 4.44, measuring heat-transfer coefficients on the RCS section that are as much as four times those near the stagnation point [46]. Figure 26 shows the heat-transfer data on both the upper and lower rays at ± 10 deg angle of attack, a value more typical of flight. The horizontal axis is the arc length from the geometrical center, normalized by the arc length to the shoulder of the blunt face. The locations of the various sections of the model are demarcated by the vertical dashed lines and indicated with text. The vertical axis is the heat-transfer coefficient. Because the model is nearly symmetric, there are near-redundant data that provide a check on the model and wind tunnel. The windward data

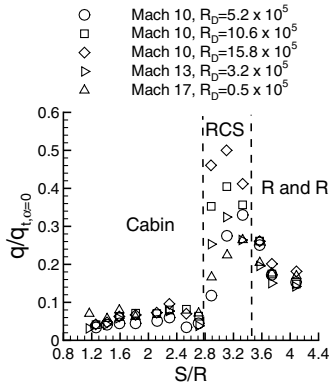

Fig. 25 Wind-tunnel heat-transfer distribution over the windward side of the Gemini afterbody at $\alpha = 10$ deg. Redrawn from [44].

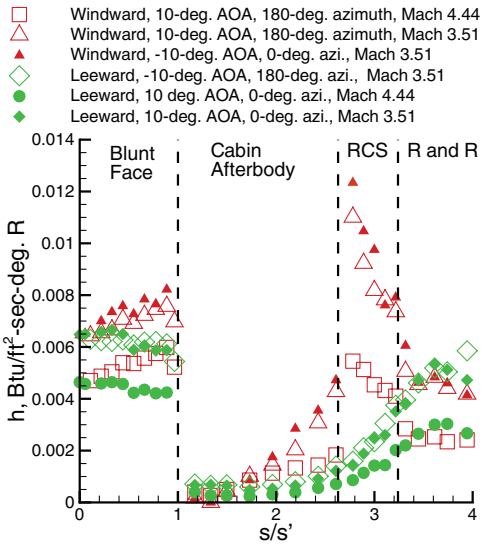

Fig. 26 Heat-transfer coefficients for Gemini reentry configuration at $\alpha = \pm 10$ deg. From Table 4 in [46].

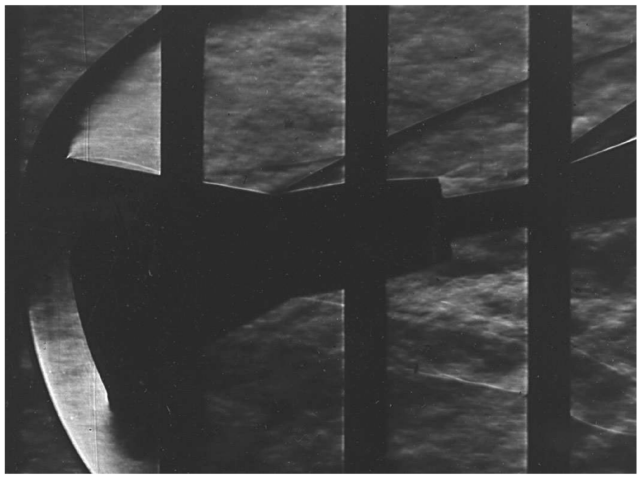

Fig. 27 Schlieren photographs of Gemini reentry configuration at Mach 3.51 and $\alpha = -10$ deg. Rescaled from Fig. 5a in [46].

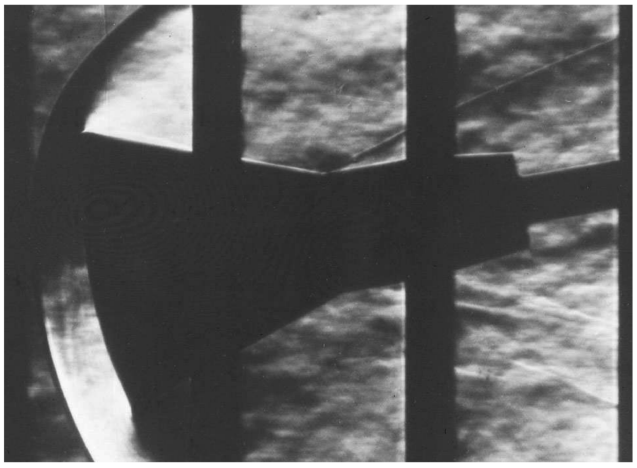

Fig. 28 Schlieren photographs of Gemini reentry configuration at Mach 4.44 and $\alpha = -10$ deg. From Fig. 5b in [46].

are colored red and the leeward data are green. The open and closed diamonds are at nominally the same conditions and repeat well; the same is true for the open and closed triangles. The separated-flow heating to the cabin afterbody is low, but rises toward the aft end. The heating suddenly rises as the flow moves on to the RCS section; the windward heating reaches nearly twice the values on the blunt face. The windward heating falls moving onto the R&R section, whereas the leeward heating rises continuously from the beginning of the cabin afterbody through the end of the R&R section.

Some understanding of these heating patterns can be obtained from the schlieren image in Fig. 27, which shows separation from the corner of the blunt face, followed by reattachment about halfway down the conical cabin section; the separated flow appears laminar, although the quality of the image seems insufficient to judge with confidence. There is a compression shock beginning at the leading corner of the RCS section. The high heating over the RCS section is presumably due to the thin boundary layer aft of the recompression shock, whereas the lower heating on the R&R section is probably because it is aft of an expansion fan (which is not really visible). The vertical bars are the window braces of the tunnel. The brightness and contrast were enhanced, using a scan of the original photo, to improve the visibility. Figure 28 shows a similar schlieren at Mach 4.44; the recompression shock is again evident, although the separation at the corner if present is washed out by the high brightness region. The other images obscure the origin of the compression shock behind a window brace. The high heating on the RCS section appears to be caused by an "interaction of the approaching cabin-section flowfield with the compression waves which are generated by the cylindrical RCS section" ([44], p. 10). It would be interesting to see if a modern computation could reproduce this complex flowfield. It seems possible that the heating patterns on the RCS section in Fig. 25 rise with distance when they are transitional and fall with distance once they are fully turbulent; however, this hypothesis remains to be confirmed.

Raper also reviewed flight data for afterbody aeroheating on the first four Gemini flights, noting in his abstract [44]:

> Transition to turbulent flow over the spacecraft during reentry occurred in several stages. Transition over the entire leeward side occurred first, following by transition over the windward side of the reentry control system and the rendezvous and recovery section. Transition over the windward side of the cabin occurred approximately 20 seconds after transition on the reentry control system and the rendezvous and recovery section.

This conclusion was supported by data such as Fig. 29, which shows heating rates for the windward side of the cabin on Gemini II. The peak laminar heating apparently occurred at about 190 s, at the same time as the peak in the calculated laminar stagnation-point heating. The second heating peak at 220–230 s was thought to be due to increased heating rates due to turbulence. The arc-length transition Reynolds numbers based on reference conditions were about 2×10^4 on the leeward side and 1.5×10^5 on the windward side. In flight, transition appears to occur two to three times later than in the wind tunnel ([44], Fig. 10b), although the wind-tunnel data are from several facilities at several Mach numbers and thus inconclusive. It would be interesting to compare the results to a modern computation.

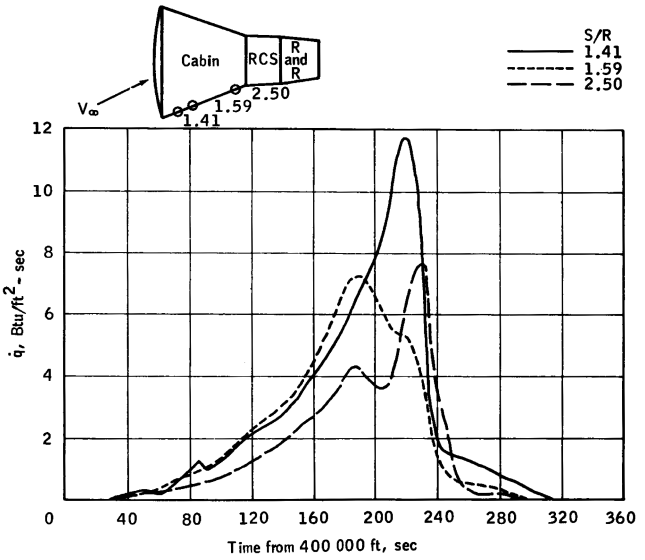

Fig. 29 Gemini II reentry heating histories. From Fig. 21a of [44].

Transition on the lee side compares well to afterbody transition on the Mercury capsule. Wright et al. point out that the leeside heating to Gemini II was about 50% higher than the windward heating, indicating leeside transition due to crossflow [16]. Raper does not discuss the aforementioned burn-through phenomena.

However, this series of events did not occur for all four spacecraft, as Raper also notes that there was no evidence of transition in the afterbody cabin heating on Gemini III and IV, which flew much shallower trajectories. The first Gemini flight did not yield any reentry aeroheating data. Although Raper does not seem to explain how the windward heating data were extracted from slow sensors on a rolling vehicle, the data seem worthy of a reanalysis with modern methods. Raper suggests that similar data should also be available for the forebody heat shield ([44], p. 5), but reports for this portion of the heating data have not yet been located. Transition was also an issue for the exit configuration ([44], p. 8).

Apollo

Introduction to Apollo Aerothermodynamics

Kruse analyzed shadowgraph images of an Apollo-like capsule in flight in the NASA Ames ballistics range [47]. The radius of the blunt face of the model was equal to the diameter, the half-angle of the afterbody was 26.5 deg, and the aft end had a radius equal to one-tenth of the diameter. As in other cases, the geometry is somewhat different than the actual Apollo capsules, which had an afterbody half-angle of 33 deg and a blunt-face radius that was 2.35 times the diameter [48]. Flow separation and reattachment on the afterbody were correlated as a function of angle of attack and Mach number. Because separation depended on transition, transition was discussed in detail, although most of the data are for laminar separation. Mach number ranged from 1 to 9, and Reynolds number based on freestream conditions and diameter ranged from 0.25 to 5 million. Many instructive shadowgraphs are shown.

Transition was correlated with the length Reynolds number from the stagnation point, independent of angle of attack; the separated shear layer was always turbulent below Mach 1.7, but otherwise stayed laminar for $Re_{2x} \simeq 2.5$–3.5×10^5 ([47], Fig. 8). Transition on the blunt face occurred for $Re_{2x} > 3 \times 10^5$ based on edge conditions, and $Re_\theta > 200$–250. Here, Re_θ is a Reynolds number based on momentum thickness and edge conditions, and Re_{2x} is a Reynolds number based on flow properties downstream of the normal part of the bow shock, and the streamline distance x from the stagnation point to the corner at the junction of the front face and afterbody. At angle of attack, the stagnation point was taken as the forwardmost point on the body.

Figure 30 shows a sample shadowgraph. The bow shock is evident, along with vertical and horizontal lines that are caused by fishing line strung in front of the windows to accurately reconstruct the position and orientation of the model when the image is taken (private communication, Dr. Michael Wright, NASA Ames, April 2005). The corners of the blunt face appear cusped due to optical distortion from the strong expansion fields. Separation is evident aft of the upper corner, along with reattachment and a reattachment shock. The flow does not reattach behind the lower corner, but forms a classic turbulent wake which is nicely imaged here.

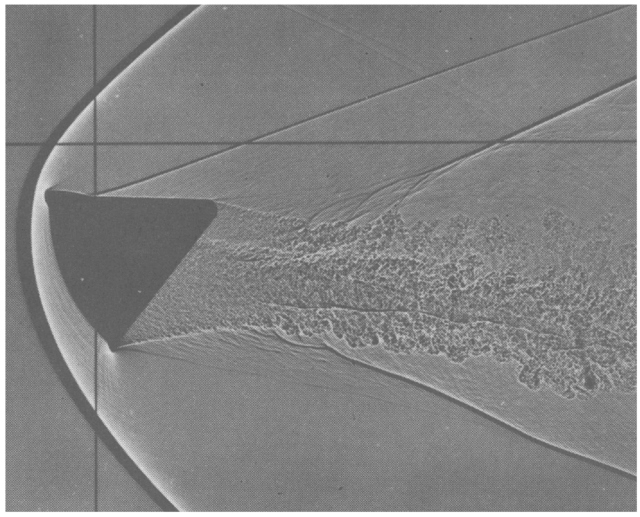

Fig. 30 Curious parallel waves near blunt face of Apollo-like capsule at Mach 2.2 and 25 deg AOA, $Re_D = 1.5 \times 10^6$. From Fig. 3d in [47].

Kruse shows four shadowgraphs at Mach 2.2 and $Re_D = 1.5 \times 10^6$ to demonstrate that the windward afterbody flow is separated at 3 deg angle of attack, and becomes attached only for larger angles of attack when it becomes more nearly parallel to the flow direction (See Fig. 30 and [47], Fig. 3). Again, Re_D is a Reynolds number based on body diameter and freestream conditions. The windward meridian was generally attached for angles of attack greater than about 12 deg at Mach 2, decreasing to about 4 deg at Mach 8. Reynolds number increased with Mach number in these plots ([47], Fig. 5). The lee afterbody flow is nearly always separated.

The flow in the separated shear layer past the corner stays laminar farther downstream as the angle of attack (α) increases. The windward separated flow at Mach 2 and $\alpha = 22$ deg stays laminar to reattachment for $Re_D = 0.45 \times 10^6$ and 1.4×10^6. However, in some cases fully attached flow occurred on the afterbody near zero angle of attack; Fig. 31 shows attached afterbody flow at slightly higher Reynolds number than the separated afterbody flow of Fig. 32 ([47], Fig. 4). Kruse believes the unusual attached flow was due to the onset of transition on the blunt face, for $Re_{2d} \simeq 3$–6×10^5 or $Re_{2x} > 3 \times 10^5$, although "turbulent flow on the face is not a

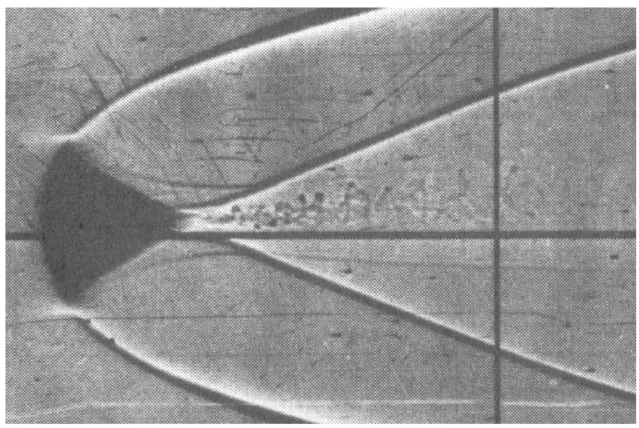

Fig. 31 Attached flow on Apollo-like afterbody at Mach 8.75 and $Re_D = 4.23 \times 10^6$. From Fig. 4a in [47].

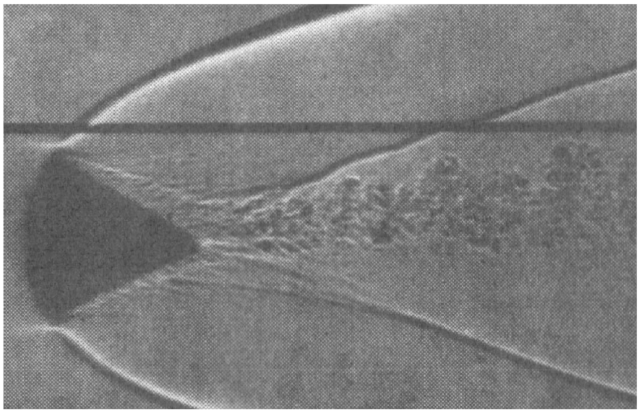

Fig. 32 Separated flow on Apollo-like afterbody at Mach 8.28 and $Re_D = 3.09 \times 10^6$. From Fig. 4b in [47].

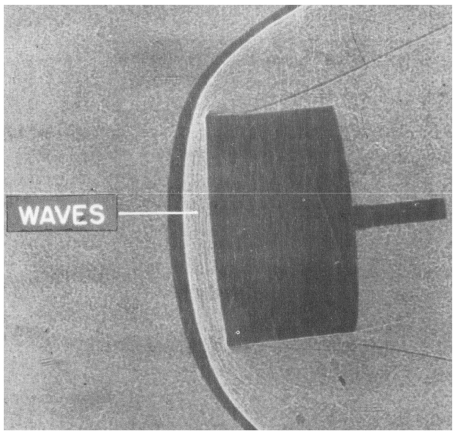

Fig. 33 Curious parallel waves near blunt face of flat-faced cylinder at Mach 8.8. From [49].

sufficient condition for attached flow on the afterbody at small angles of attack." Here, Re_{2d} is a Reynolds number based on body diameter and conditions behind the normal portion of the bow shock. Transition on the blunt face was believed to begin on the leeward meridian. Kruse also looked at the effects of roughness on the blunt face.

Figure 30 also shows unusual waves parallel to the bow shock, between the bow shock and the model. These have never been explained, to the author's knowledge. Similar waves are also observed in [49], as shown in Fig. 33 and in Fig. 10. Canning et al. present a full-paragraph discussion of these waves; if they are compression waves from the surface traveling at the speed of sound, Canning et al. estimate their frequency as 3 MHz, which would explain why they are seldom observed. This very high frequency is also thought to rule out interaction with elastic waves in the solid model, because it is 30 times higher. It seems possible that these waves might relate to the unexplained oscillations in gas-cap radiation reported in [50], Fig. 6. The oscillations were picked up by high-frequency photomultiplier tubes with an amplitude of about 5–10% of the mean and a frequency of about 1 MHz.

Figure 34 shows a shadowgraph of an Apollo-like capsule from earlier measurements in the NASA Ames ballistic range [51]. This model again has an afterbody half-angle of 26.5 deg and a blunt-face spherical radius equal to the diameter. The Reynolds number is based on freestream conditions and the body diameter, and the speed given is relative to the freestream. The bow shock position is distorted relative to the forebody due to the shock lensing. The flow separates from the lee afterbody and forms a wake, with recompression shocks aft of the wake neck. The windward flow often separates and usually reattaches, sometimes transitioning to turbulence ([51], Fig. 13). The images in an original paper copy of the document are of good quality,

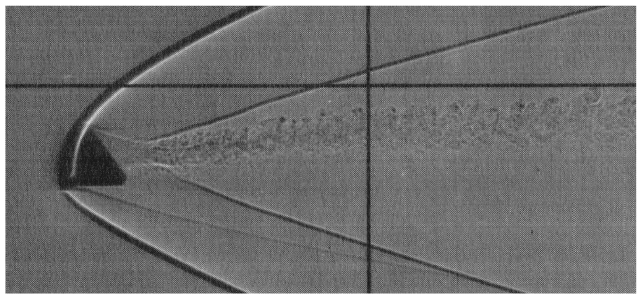

Fig. 34 Shadowgraph of Apollo capsule at 27.0 deg AOA, $Re_D = 0.49 \times 10^6$, and $V_\infty = 3760$ ft/s. From Fig. 12b in [51]. Background hatching which may appear is a printing artifact.

although details near the small model are difficult to make out. The scanned image in the present paper is of lesser quality.

Transition may occur on the forward face, or on the wind or lee sides of the afterbody. The flow was attached to the windward side at larger angles of attack, depending on velocity and Reynolds number (which varied together, as the model size and range density were held constant). The windward side was laminar for intermediate $Re_D \simeq 0.3$–0.6×10^6, depending on angle of attack, and transitional for both larger and smaller speeds ([51], Fig. 13). The unusual appearance of transition at low and high Reynolds numbers was attributed to Mach number effects.

It would be very valuable to see the original shadowgraph photographs, of which many were taken; however, the original range archive was apparently destroyed (Gary T. Chapman and James O. Arnold, private communication, Feb. 2005), so the only remaining images are those found in original paper copies of the reports, those that might have been retained privately, and those available from the NASA Ames photo archive, which apparently retained many of the images presented in the NASA reports (the ones numbered using the format A-00000).

Apollo Trajectories and Aerodynamics

General Issues

Crowder and Moote [52] review the aerodynamics of Apollo following the first four flights. Apollo was a lifting capsule, where the angle of attack was determined by an offset center of gravity. Roll control was used to modulate the lift direction to provide control of cross-range and downrange, to enable shifting the landing position if required by weather. Lift was also needed to widen the corridor of allowable entry flight-path angles from about 0.6 deg to about 2 deg. Smaller angles cause skipout and loss of vehicle, and are alleviated by an entry with the lift-vector pointed earthwards. Larger angles result in excessive g-loads and are alleviated by upward lift. An L/D of about 0.3 was used. The cross-range capability was about 200 nm, whereas the downrange could vary by about 2500 nm. The small L/D of Apollo was sufficient to provide acceptable reentry corridors and to adjust to bad weather at the landing site, but not nearly sufficient to permit much choice regarding landing sites [53]. Unlike Mercury and Gemini, Apollo *required* L/D to achieve safe reentry with acceptable margins [53].

Preflight predictions showed L/D increasing with Mach number, whereas it actually decreased during flight ([52], Fig. 10). The difference was about 0.05 or 15% at Mach 36. The cause of the difference was not known, and the flight data were used to provide improved predictions for later flights. Flight L/D seems to correlate with velocity and not Reynolds number, suggesting that real-gas effects may be the cause.

Crowder and Moote [52] show that lift is critical even for capsules, and that predicting the landing point and the reentry margins requires accurate knowledge of the aerodynamics, which is not trivial. Obtaining the aerodynamics from flight is very expensive, which may justify a ground-based risk-reduction effort, which might or might not involve transition.

The Apollo 11 flight actually used the command module lift to shift the splash point to avoid weather [54]. This was critical to safety, because the thunderstorms at the original landing location were intense enough to destroy the parachute, capsule, and astronauts [55]. The splash point was moved 215 miles downrange to the secondary recovery point, using a skip maneuver [54] (207 miles according to [53]). The peak acceleration was about 6.5 g. The recovery forces found the vehicle about 4 min of latitude (roughly 4.6 miles) away from the predicted splash point ([54], Fig. 13.1), although NASA computed a landing only about 1.7 miles from the predicted point ([54], p. 8-8). It is clear that by this flight the splash point could be controlled fairly accurately.

Specific Issues

Hillje reviews the entry flight data from Apollo 2 (spacecraft 011, mission AS-202) [56]. The wind-tunnel data had to be corrected to flight conditions to account for protuberances, center-of-mass shifts due to RCS usage, and changes in spacecraft shape due to ablation. The Reynolds number rose through about one million as the Mach number dropped from hypersonic to supersonic. The preflight predictions of trim angle were about 4–8 deg below the flight values of about 18–20 deg ([56], Fig. 8). The wind-tunnel data for the forces seem to be nearly correct, for the wind-tunnel and flight data for lift-to-drag ratio agree well when the flight-derived values of angle of attack are used. The wind-tunnel predictions of trim angle were substantially in error; the reason was not discussed.

Hillje's review of the flight data from Apollo 4 (spacecraft 017, mission AS-501) finds similar difficulties at superorbital speeds [57]. The moment predictions were again poor at high Mach numbers, possibly because of heat-shield ablation, protuberances, or some other effect. Viscous effects are not mentioned, although it seems possible that the afterbody shear layer might contribute to the trim problem. The lift-to-drag ratio differed by 10% between wind tunnel and flight, with the trim angle differing by about 1.5 deg. The Reynolds number reached about one million at hypersonic speeds.

Griffith and Boylan [58,59] analyze aerodynamic data from Apollo, and compare the flight data to wind-tunnel measurements at AEDC. The actual 3-D as-measured preflight heat-shield shape, complete with variations due to pads, etc., was tested under cold flow conditions for the first time. Earlier tests were carried out only with an axisymmetric approximation to the preflight heat-shield shape. Figure 8 in [58] shows that the wind tunnel moment coefficients scatter when plotted against Re_{2d}, but make a consistent pattern when plotted against freestream Mach number. The reason is unknown. Figure 15 in [58] shows that the trim angle of attack measured in the wind tunnel agrees well with flight when the actual preflight 3-D wavy heat-shield model is used, but differs by about 2 deg when the axisymmetric smooth model is used. Griffith and Boylan [59] state that a preflight error in the trim AOA of 3.5 deg caused a downrange splashdown error of 205 nm, for flight AS-202. Figure 16 in [58] shows that L/D agrees with flight for both heat-shield models, differing from preflight predictions by about 10%. Because the agreement is good, real-gas effects were not thought to be important. However, this argument is weak, because the agreement may be fortuitous: other effects such as the effect of ablation on the heat-shield shape may have canceled out the real-gas effects. Viscous effects were clearly important at high altitudes (above 220 kft).

Hillje and Savage [60] analyze the flight data and agree that preflight predictions of the trimmed angle of attack for Apollo were significantly in error. However, Hillje and Savage correlate the flight data to suggest the opposite conclusion, that the error is dominated by real-gas effects, and that viscous interactions are *not* important. Clearly, the flight data should be reanalyzed with modern methods to resolve the cause of the discrepancy.

Graves and Harpold [61] review mission planning and targeting for Apollo entries. The guidance logic was developed to reach the splash point despite uncertainties in the aerodynamic properties. The greatest difficulty was due to changes in mission requirements as downrange specifications changed due to other mission issues. Originally, the downrange manuevering capability was to be 3500 nm so that the earth landing point could always be at one of two target points. This later had to be relaxed to 1000 nm because insufficient L/D could be achieved. This change caused difficulties with the control system development ([61], p. 20). This remark makes clear that the landing specifications for the CEV will be a dominant factor in the aerodynamics required. What will the mission scenario be? Must the vehicle always land at a single land-based location? Are a range of land-based locations to be permitted? What requirements will be set in terms of time-to-land from an arbitrary initial condition, allowable g-loads, and so on? It is clear that these kinds of specifications are critical. Harpold [62] discusses the specification for minimum L/D during the Apollo program, to ensure capture and sufficient downrange control under various guidance-system failure assumptions; 0.3 was thought to be the minimum. Because transition affects trim and drag, requirements for L/D affect the importance of transition. See [63] for a discussion of these issues regarding the mission of the X-38 lifting-body vehicle; note there that transition is clearly critical for lifting bodies and winged vehicles.

Bell Communication Company [64] analyzes the effects on mission planning of a reduction in reentry range from 5000 to 3000 nm. The original landing sites in Australia and South Texas became unfeasible as Apollo analysis proceeded. The ability to land depends on many factors, including time of the month, service-module propellant usage, latitude of the landing site, reentry range limits, reentry flight-path angle, and time of flight. Reducing the feasible reentry range narrows the other choices. Propellant carried on the service module is very expensive mass. Limiting the possible landing conditions may become a safety issue in the case of abort scenarios. One of the best arguments for research in aerothermodynamics may be the increase in landing flexibility and safety that could result from higher L/D. It is interesting to note that Apollo was originally designed to come down on land ([65], p. 18).

Apollo Aeroheating

Introduction and Preflight Assessments

Erb et al. [66,67] review the development of the Apollo TPS. Although the Mercury capsules used reradiative metallic shingles for the afterbody TPS, this was thought to be risky due to the difficulty of predicting aeroheating in flow reattachment areas, leading to the choice of an ablating afterbody TPS. Here, more advanced analyses might enable the use of a reusable afterbody TPS, possibly making the vehicle more reusable, requiring only the replacement of the blunt heat shield. No other viscous-flow-related aerothermodynamics issues were evident in this excellent overview written by the program managers.

The North American Aviation staff ([68], pp. 4–5) summarize the preflight predictions for transition on Apollo, according to the vehicle contractor. Transition was expected at an arc-length Reynolds number $Re_x \simeq 150,000$; expected transition times were tabulated. Transition in the wake was assumed to occur at a Reynolds number of $Re_x \simeq 20,000$. The effect of transition on the TPS design is not discussed.

Lee analyzed the effect of transition and trajectory on the heating to the Apollo command module, preflight [69]. Most of the peak heating is radiative, but for the shallower trajectories most of the total heat load is convective. Transition was again expected at a local Reynolds number of 0.15×10^6, here per [70]. Lee goes on to comment that "transition was observed at a Reynolds number of 20,000 in a separated region on the Mercury spacecraft conical section," citing [71], and notes that this implies that transition could begin early in the reentry on the leeward conical section of Apollo. Because [70,71] are still limited distribution, they will not be further discussed in this paper. Lee analyzes the worst-case effects of turbulence in her Fig. 10, but the legend in the graph seems to be flawed and the graph is hard to understand. A reanalysis appears to be in order.

Ground Tests

Jones measured the heat transfer on the blunt face of an Apollo-like model in the Langley Mach-8 variable density tunnel [72]. Thin-skin calorimeter methods were used. The two-page note shows heat-transfer data on the face of the capsule. At the highest Reynolds number of $Re_D = 3.8 \times 10^6$ based on capsule diameter and freestream conditions, the nondimensional heating rate suddenly rises about halfway along the heat-shield surface. The author attributes this rise to transition, which occurs at a length Reynolds number of about 200,000, only for angles of attack between 20 and 32.5 deg. This paper is evidence for transition on the blunt face of such a capsule, but the data are very limited and more information is needed; for example, the model diameter is not given. Although no further information on these transitional forebody measurements could be found, Jones earlier measured laminar flow on a 4-in.-diam blunt face in the same tunnel at Mach 8 and $Re_D = 1.4 \times 10^6$ [73]. Jones also plots simple theoretical estimates, suggesting that transition would increase the heating to the blunt face by factors of 2–3 at 180 kft and 32 kft/s or 155 kft and 30.5 kft/s.

Jones made heat-transfer and flow visualization measurements on the Apollo afterbody in Mach-8 wind-tunnel tests [74,75]. Figure 35 shows an oil-flow image of the separation that occurs just aft of the shoulder of the blunt face. The entire afterbody flow appears to be separated, as was confirmed by tufts and movies of small oil drops injected through afterbody pressure taps. At high angles of attack near the 35-deg afterbody half angle, the flow becomes attached on the windward afterbody, as shown in Fig. 36. Intermediate angles of attack are not discussed; note that the afterbody half-angle differs somewhat from the final flight value of 33 deg. Jones obtained schlieren images of the flow, but the shear layer is not visible, even in original copies, illustrating the difficulty of obtaining high-resolution schlieren in wind tunnels at low densities.

In preliminary tests at the maximum Reynolds number of 1.36 million based on freestream conditions and body diameter, Jones observed a possible indication of transition via increased heating rates towards the end of the windward afterbody ([74], Fig. 2a). The sting used to support the model had some effect on the afterbody measurements, in a way which was clear yet difficult to quantify, reducing confidence in the results. Jones ([75], p. 10) believed that sting interference caused the increase in heating with downstream distance at the highest Reynolds number and zero angle of attack. This increase varied with azimuthal angle even at zero angle of attack, and was reduced by placing small roughness elements just upstream of the separation point; qualitative images with temperature-sensitive paint seemed to confirm the interference problem. The experiments show the difficulty of making afterbody measurements in a wind tunnel with normal support techniques. Jones believed his flow was laminar except possibly when tripped by the small roughness. "The effectiveness of this roughness in promoting boundary layer transition was not determined" ([75], p. 10).

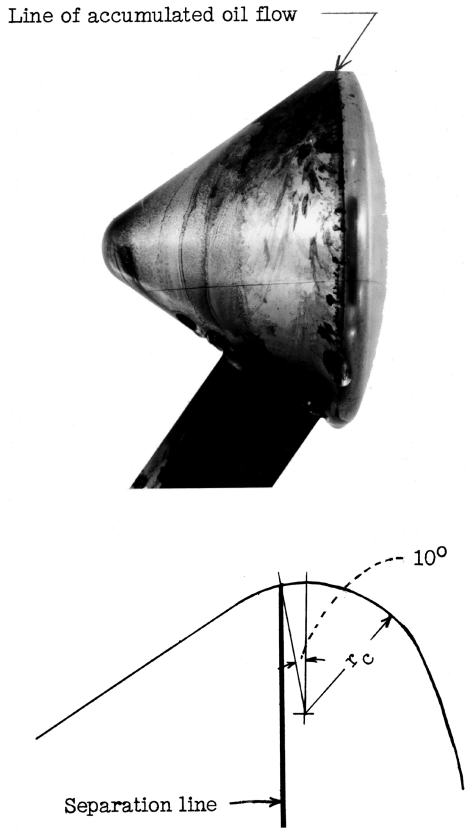

Fig. 35 Photograph and sketch of oil-flow pattern on Apollo at zero AOA and Mach 8, showing separation. Flow from right to left. From Fig. 6 in [75].

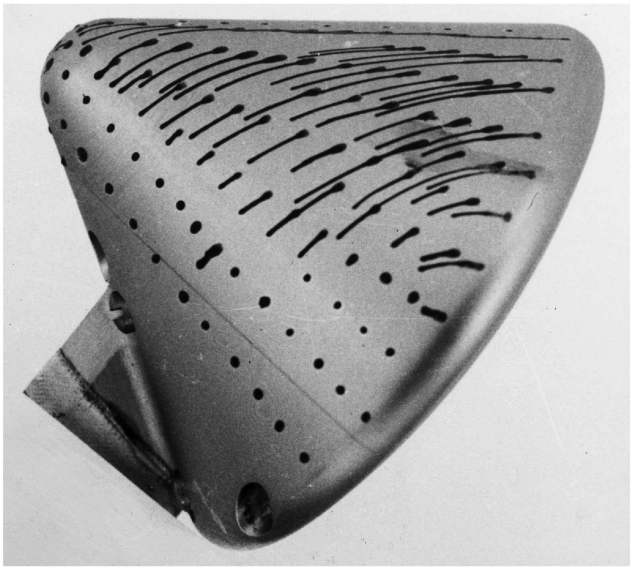

Fig. 36 Photograph and sketch of oil-flow pattern on Apollo at 35 deg AOA and Mach 8, showing lee separation. Flow from right to left. From Fig. 9 in [75].

Jones measured heat transfer to the afterbody of the Apollo reentry vehicle in a shock tunnel at NASA Langley [76]. The measurements used methods that were still under development at the time, so the quality is limited. The afterbody heating levels were below those measured in a conventional wind tunnel at Mach 8 [75], for unknown reasons. Consistent asymmetries in the azimuthal distribution of afterbody heating rates were tentatively attributed to small flaws in the joint between the forebody and afterbody, which suggests the importance of issues related to boundary-layer separation and transition.

Marvin et al. measured pressure and heating distributions to the blunt face of an Apollo model in the Mach-20 helium tunnel at NASA Ames [77], at $Re_D = 1.85 \times 10^6$. The heating rates remained near or below Lees's laminar boundary-layer theory [78], so the boundary layer was thought to be laminar. The good-quality oil-flow images show flow moving radially from an axisymmetric stagnation point near $\alpha = 0$; as AOA increases, the originating point becomes an originating line and moves windward.

Marvin and Kussoy then measured afterbody pressure and heating distributions on an Apollo model in the Mach-20 helium tunnel at NASA Ames [79], at $Re_D = 1.85 \times 10^6$. The flow over the windward meridian was attached for $\alpha > 20$ deg, and separated for $\alpha < 15$ deg; the afterbody half-angle of 33 deg again matched the flight vehicle. The afterbody heating rates were in fair agreement with simple theory for laminar separated flow. The separation was visualized with the oil-flow and glow discharge techniques, at various angles of attack. Figures 37–39 show front, plan, and side views of the oil flow near the operating vehicle angle of attack. On the blunt face (Fig. 37), the flow moves radially from a stagnation region

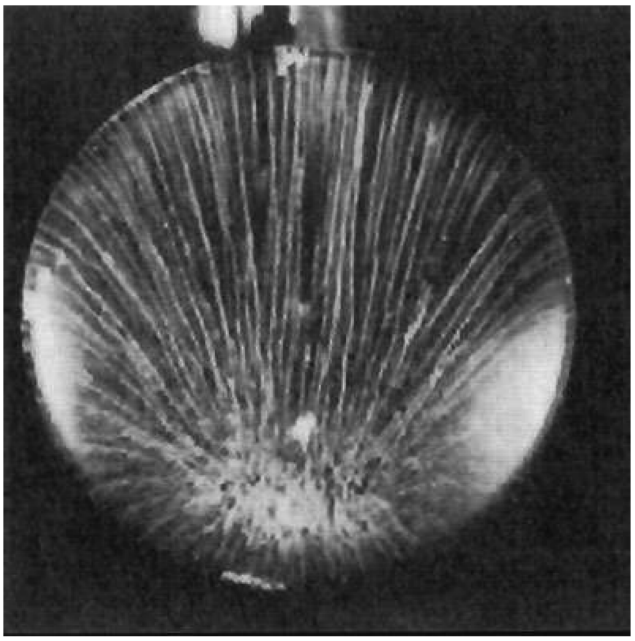

Fig. 37 Oil-flow patterns on the Apollo afterbody in helium at Mach 20. Front view at 25 deg AOA. From Fig. 2a in [79].

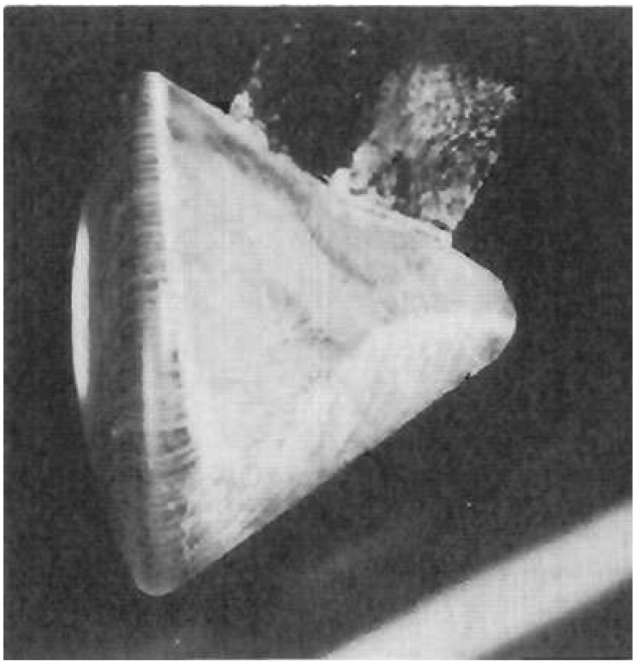

Fig. 39 Oil-flow patterns on the Apollo afterbody in helium at Mach 20. Side view at 25 deg AOA. From Fig. 2a in [79].

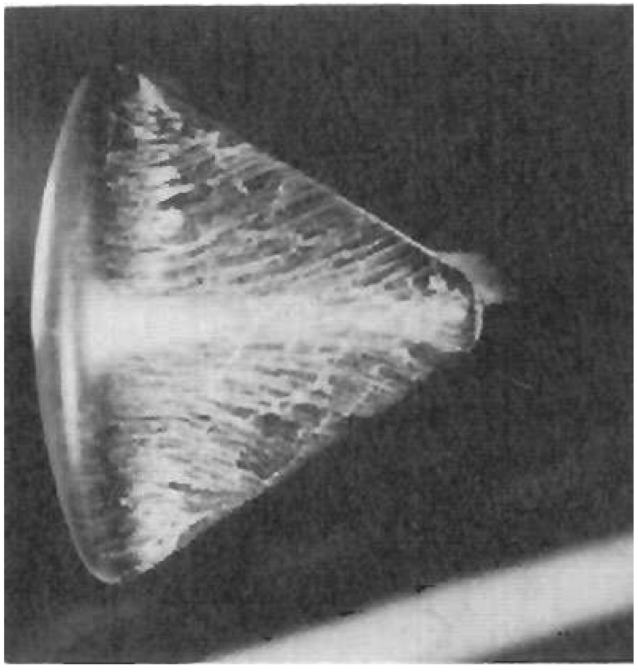

Fig. 38 Oil-flow patterns on the Apollo afterbody in helium at Mach 20. Plan view at 25 deg AOA. From Fig. 2a in [79].

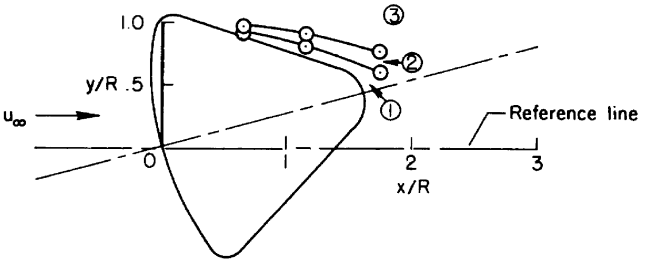

Fig. 40 Location of separated shear layer relative to the Apollo afterbody in helium at Mach 20. Fifteen-degree AOA near windward meridian. From Fig. 4b in [79].

on the windward side that appears to be a line. The flow is attached in the windward afterbody plan view (Fig. 38). The image from the side (Fig. 39) is less clear, but seems to show attached flow over much of the windward side. The lee side separates just past the rounded edge from the blunt face. The side-mounted strut support is visible on the upper aft portion of the model in Fig. 39.

Pitot profiles were also measured, in the separated afterbody region at $\alpha = 0$, 15, and 33 deg. Although the resolution was not nearly good enough to resolve the attached boundary layer, the location of the separated shear layer was readily plotted with respect to the body, as shown in Fig. 40. Region 1 is the separated flow near the afterbody, region 2 is where the pitot pressure varies markedly due to shear, and region 3 is where the pitot pressure varies slowly due to outer-flow inviscid effects. The pitot-pressure results confirmed the qualitative evidence of the glow visualizations. Although the data are in helium, and thus have an uncertain relation to earth reentries, it should be possible to reproduce the experiments with modern numerical techniques. A good comparison with CFD in both air and helium might improve confidence in CFD simulations for reentry to other planets with different atmospheres.

Lee correlates the wind-tunnel aeroheating data for the windward afterbody of Apollo [80]. The data from Ames, Langley, and Cornell all correlate with Stanton and Reynolds numbers. The data mostly fall below a simple laminar flat-plate theory, indicating separation. However, at 33 deg angle of attack, when the windward ray is aligned with the flow direction, the data correlate well with the flat-plate theory.

Bertin et al. summarized the experimental aeroheating data for Apollo, preflight [81]. The Reynolds number of the ground-test data was generally too low to see transition, with the exception of a single shock-tunnel run ([81], p. 9). This is probably because of the need to use small models when trying to start a supersonic tunnel with such large bluntness. $Re_k \simeq 400$ was used to infer that roughness on the flight vehicles would be much less than the 0.695 in. thought necessary to affect transition. Here, Re_k is the usual roughness Reynolds number based on the roughness height k and conditions in the undisturbed laminar boundary layer at the roughness height. Note that values of Re_k of 25 or less have been used by others to determine roughness heights small enough to have no effect on transition, so there is considerable uncertainty [82]. Bertin's inferences were supported by limited wind-tunnel data (one figure is given at Mach 10.19 in an unspecified wind tunnel).

Bertin also summarized the wind-tunnel data for protuberance and cavity effects [83]. However, this later paper contains no information regarding transition. Similarly, Mosely and Martino reviewed the entire Apollo wind-tunnel program, mentioning heat-transfer measurements in AEDC tunnels A, B, and C, and in the Cornell shock tubes ([84], p. 32). However, there are no references to specific physical features regarding the trim moments or the aeroheating. The tunnels that presently form the Langley hypersonic facilities complex were not used in developing Apollo, possibly because they were not operational in time.

Yee measured afterbody heating rates in the ballistic range, and finds that they dropped by a factor of 2 when the heat shield was ablating [85]. This observation may support some of the inferences regarding ablation effects that are presented next.

Flight Results

Pavlosky and St. Leger review the thermal-protection system for Apollo [65]. Tables 2 and 3 in the report summarize the various Apollo flights, giving flight-path angles at entry, entry speeds, maximum heating rates, and so on. The crew preferred downrange distances of 1500 nm, which corresponded to integrated heating of $26,500\ \mathrm{Btu/ft^2}$; these were much shorter than the Block II requirement for 3500 nm downrange which resulted in integrated heating of $44,500\ \mathrm{Btu/ft^2}$. The cause for the preference is not specified. Flights 8–16 had downrange distances of 1184–1295 nm, except for Apollo 11, which flew 1497 nm downrange. The maximum reference heating during operational flights was $27,939\ \mathrm{Btu/ft^2}$, much less than the $37,522\ \mathrm{Btu/ft^2}$ on the AS-501 test of spacecraft 17. Thus, the TPS had lots of margin, for typical flights. The TPS weight was a major consideration during the program, and a boost protective cover was added to remove ascent heating and reduce entry weight. The original plan was to come down on land. Clearly, TPS weight and system design is heavily influenced by the selection of entry trajectories and design margins.

Lee reviews the aerothermodynamics experience on Apollo [86]. Spacecraft 009 and 011 reentered at orbital velocities, with 009 having a Reynolds number three times higher than the others due to a steeper entry angle ([86], p. 6). Spacecraft 020 and 017 reentered at superorbital velocities. Details relative to transition are not presented in this overview report.

Lee et al. analyzed heat-transfer and pressure measurements on the Apollo command module during the orbital reentry test flights [87]. Apollo Missions 1 (Spacecraft 009) and 3 (Spacecraft 011) are discussed in detail, and analyzed with simple correlations a la Van Driest. Transition was expected to occur at $Re_x = 1.5 \times 10^5$ in attached flow and $Re_x = 2.0 \times 10^4$ in separated flow. The blunt "aft" face is a spherical segment with a radius of 184.8 in.; it is faired into the conical crew compartment using a toroidal section with a 7.7-in. radius. The maximum body diameter is 154 in., and the half-angle of the crew compartment is 33 deg [48,87].

Apollo 1 reentered through 400 kft. at $25,173\ \mathrm{ft/s}$ and a flight-path angle of -9.03 deg [87]. The altitude reached a minimum at about 135 kft and 15 kft/s, skipped up, and then descended to a landing. The Reynolds number history was not plotted. Apollo 1 suffered an electrical malfunction and the loss of all heating-rate data at 86 s after entry. The angle of attack was 19.7 to 21.3 deg until 83.4 s after entry, when it began rolling rapidly. The pressure distributions measured in flight agreed well with predictions based on the wind-tunnel data, except behind the scimitar antenna. Six of the calorimeters on the blunt face were partially operational during the reentry, but the data were insufficient to infer reliable heating rates. There were thus no useful data from the blunt face. The heating on the windward afterbody conical section rose well above the simple laminar theory ([87], Figs. 16a, 16b, 16d), and agreed well with the simple turbulent theory well downstream of the scimitar antenna (Lee's Fig. 16d), leading Lee et al. to infer the onset of transition at $Re_x \simeq 4.0 \times 10^4$. The heating on the toroidal section showed some evidence of a slope change that was associated with transition at $Re_x \simeq 3.0 \times 10^4$. The heating on the leeward afterbody conical section showed evidence of transition on several sensors (Lee's Figs. 16j–16p), at roughly 1630 s, just before the first altitude minimum. Transition Reynolds numbers were estimated to be $Re_x \simeq 4.0\text{–}10.2 \times 10^4$, but laminar flow was observed at some stations to $Re_x \simeq 2.7 \times 10^5$. The data should be reanalyzed with modern computational methods.

Apollo 3 reentered at $27,200\ \mathrm{ft/s}$, a flight-path angle of -3.53 deg, and an angle of attack of 18 deg [87]. The altitude reached a minimum at about 210 kft., 25 kft/s, and $Re_D \simeq 0.3 \times 10^6$, skipped up, and then descended to a landing. The Reynolds number rose through one million at about Mach 10, late in the landing trajectory. The pressures measured in flight again agreed well with the preflight predictions. The thermal sensors on the blunt face again failed in reentry and no useful data were obtained. The low heating rates suggested separated afterbody flow. The angle of attack rose to 20 deg during entry, "which may have caused the flow to attach to the windward conical section after the peak of the second heating pulse" ([87], p. 9). The heating rates on the windward afterbody generally depart from simple laminar predictions at about 4800 s ($Re_D \simeq 0.3 \times 10^6$), reaching simple turbulent predictions at about 4900 s ($Re_D \simeq 0.7 \times 10^6$) (Lee's Figs. 17a–17e). Away from the windward ray, the heating departs from laminar later in the flight, in an irregular fashion, which might possibly be associated with intermittent transition or reattachment. Lee et al. inferred transition onset at $Re_x \simeq 20\text{–}102 \times 10^3$, possibly depending on three-dimensional effects. Again, the data should be reanalyzed with modern computational methods if possible; one such recent analysis was performed by Wright et al., who inferred transition at several aft thermocouples for this flight [16]. The lack of heating data on the blunt face in the orbital flights is a major loss.

Lee and Goodrich also analyzed the superorbital test flights [88]. Apollo 4 (Spacecraft 017) reentered at $36,628\ \mathrm{ft/s}$, and Apollo 6 (Spacecraft 020) reentered at $32,830\ \mathrm{ft/s}$, below the planned velocity due to a rocket failure. Both spacecraft were trimmed to reenter at a 25 deg AOA ([88], p. 5). The spacecraft again reentered, skipped up, and landed. For Apollo 4, $Re_D \simeq 1.2 \times 10^6$ during peak heating at the first altitude minimum, at about 180 kft and Mach 28. For Apollo 6, $Re_D \simeq 1.1 \times 10^6$ during peak heating at the first altitude minimum, at about 190 kft and Mach 26. The pressures on the blunt forward face (which is called "aft," from the launch perspective, in much of the Apollo literature) agreed well with preflight predictions for both spacecraft. However, the pressures on the afterbody near peak heating were about $1/3$ of preflight predictions for Apollo 4, and about $1/2$ for Apollo 6. The afterbody heating rates were also correspondingly low. The differences were attributed to mass injection from ablation, in part because the differences were larger for the higher speed flight. However, it also seems possible that the differences are related to boundary-layer separation and transition.

Turbulent heating to the blunt "aft" face (which faced into the flow at reentry) was computed with a simple flat-plate theory ([88], p. 7). Transition was originally predicted at $Re_x = 150,000$ in attached flow and $Re_x = 20,000$ in separated flow, but the orbital flight data of [87] were used to justify a new attached-flow transition estimate of $Re_x = 80,000$. No turbulence was expected on the afterbodies of Apollo 4 or 6, due to the low Reynolds numbers computed there.

The wafer calorimeters on the blunt face were redesigned following the complete loss of data on the orbital flights, and could be calibrated only postflight ([88], p. 8). The sensors became erratic above 2000°F near the peak heating point; this results in a major limitation in determining if the peak heating was turbulent or not. The data were in general thought to agree with laminar convective heating rates corrected for blowing effects, although the computational methods are crude by modern standards.

The temperatures on several calorimeters on the blunt face of Apollo 4 show multiple peaks near peak heating; Lee and Goodrich seem to attribute these to sensor problems, but it also seems possible that they may be related to transition ([88], Fig. 13). Lee and Goodrich indicate an Apollo-4 transition point near 30,100 s for the sensors on the blunt face at $Y_c = 12.7$ in. and $Z_c = -49.5$ (off centerplane) and at $Y_c = -4.74$ in. and $Z_c = -50.0$ (on centerplane at $S/R = -0.663$); however, these markings on Lee and Goodrich's

Figs. 13a and 13c are not explained in the text. Here, S is arc length from the stagnation point, R is the radius of the blunt face, and Y_c and Z_c are distances from the geometric center of the blunt face. Transition was expected on the sensor at $S/R = -0.663$ per Lee and Goodrich's Fig. 14f, but the predicted increase in heating rate is not shown and the measurements end at 30,150 s, before transition onset. Similar results are shown for two other blunt face sensors in Lee and Goodrich's Figs. 14g and 14h.

The temperatures on the blunt face of Apollo 6 also show multiple peaks near the peak heating period ([88], Fig. 15). The heating rates for the sensor near the center of the blunt face at $S/R = 0.004$ are predicted to rise rapidly with transition near 34,800 s, but the sensor data end at 34,780 s. Several other sensors show similar behavior. The sensors on the blunt face in Lee and Goodrich's Figs. 16b and 16c show marked rises near 34,770 s that do not agree with the simple predictions and may be due to transition. For the sensor in the middle of the lee side of the blunt face, at $S/R = -0.663$, Lee and Goodrich's Fig. 16f shows a sudden rise in heating near 34,780 s that they associate with transition, possibly in agreement with Fig. 41, but the sensor data end at 34,780 s, right at the beginning of the predicted rise.

Bartlett et al. reanalyzed sample flight data from the Apollo entry vehicles using fairly modern techniques that were newly available at the end of the Apollo era [89–91]. Although in 1970 the pressure distribution was still obtained from wind-tunnel data, the boundary layer was computed using an early version of the BLIMP integral-matrix code, and the surface ablation was accounted for using a one-dimensional heat conduction code including pyrolysis. Radiative heating was also accounted for. The computations gave good agreement for the laminar flow cases, enabling the clear detection of transition in these complex flows.

Figure 41 shows transition onset at $s/R = -0.663$ on the leeward meridian of the blunt face of Apollo 6 (command module 020) during the initial high Reynolds number heat pulse, at 25 deg angle of attack. Here, s is the distance along the streamline measured from the geometrical center of the blunt Apollo heat shield (radius R); this sensor is roughly halfway between the geometric center and the edge of the blunt face. The net heating rate is due to convection plus incident radiation, and Bartlett et al. tabulate the boundary conditions used ([89], Table 21). Transition clearly occurs on the blunt face, and clearly has a major effect on the net heating rate. The flight data published here are from a private communication from W. Goodrich at the Manned Spacecraft Center, who apparently reanalyzed some of the marginal data from the thermal sensors on the blunt face ("These data and NASA/MSC predictions were supplied by MSC personnel and differ somewhat from the values reported in the Apollo mission reports" [89], p. 170.) Transition onset at the 66 s shown also yields computed heat-shield temperature distributions in good agreement with the in-depth thermocouples (see [89], Fig. 46). Bartlett et al. believed that the flow returned transitional at 115 s and laminar at 136 s, judging from comparisons to the in-depth thermocouples. During the 40 s of fully turbulent flow, the turbulent heating was estimated to be three times the expected value for laminar flow.

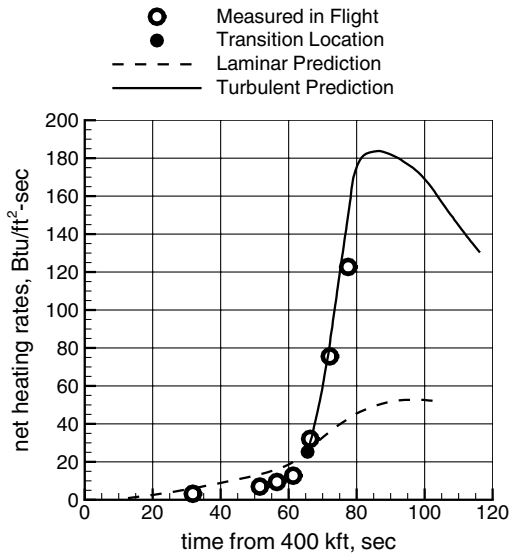

Fig. 41 Comparison of predicted heating rates with wafer calorimeter data for body point 707 on Apollo-6 flight AS-502 (Spacecraft 020). Redrawn from Fig. 66a in [89].

Bartlett et al. also provide computations indicating transition at the same body point on the blunt face (their Figs. 66b and 47) and on the afterbody heat shield (their Fig. 69) for flight AS-501 (Apollo 4). Although Bartlett et al. provide good evidence for the occurrence of transition on Apollo, a modern reanalysis of this data is needed to confirm and extend these early results.

Later Reanalysis

Williams et al. analyzed Apollo reentry shapes using fairly modern methods to aid design of future lunar-return vehicles [92]. They state, "Turbulence for Apollo occurred late in time and would not affect the TPS sizing." However, this statement is not supported by a reference or any data. Bouslog has commented that it was thought that the windward heat shield dominated the heat-shield weight, and that the total heat load to the windward heat shield was dominated by radiative heating and laminar convective heating (private communication, April 2005). The analyses were apparently carried out assuming laminar heating, and afterbody heating analysis methods are not discussed. No comparisons to flight data are shown. Although it may well be that turbulent heating is not a major issue for future manned capsule designs, this has not yet been shown in any published analysis known to the present author. In particular, because CEV capsules are to be substantially larger than Apollo, the Reynolds numbers are likely to be higher, and transition seems more likely to be an issue.

Wright et al. performed a modern analysis of the afterbody heating rates on the Apollo-3 reentry (AS-202) [48], using a full finite-rate-chemistry Navier–Stokes code. As discussed earlier, Lee et al. [87] believed that several thermal sensors on this flight showed higher heating levels due to transition. Wright et al. suggest that two windward afterbody sensors ("c" and "d") may show attached transitional flow during the second heating pulse. In addition, several calorimeters in the separated afterbody region may also show transitional or turbulent flow during the second heating pulse (see also [16]).

Planetary Probes

Galileo and Pioneer-Venus

Park and Tauber review heatshielding problems for planetary probes [93]. They use transition to explain the higher-than-expected heating rates that occurred downstream of the stagnation point for Galileo, and for the Large, North, and Night Pioneer-Venus probes. Temperatures reached twice the preflight predictions on the Pioneer probes, and the frustum recession was twice the prediction for Galileo. A detailed analysis of various computational comparisons is given (see also [94,95]). It is clear that many uncertainties remain in the computation of these high-enthalpy flows with chemistry, ablation, radiation, roughness, spallation, and transition. Park and Tauber give a good argument for including transition as part of a risk-reduction analysis for these heatshields. A less conservative analysis would enable reducing heat-shield mass.

Mars

Viking Era

Zappa and Reinecke measured heating to the afterbody of typical Mars entry shapes, using a shock tunnel [96]. The models were suspended from wires and instrumented with thin-film gauges. The test gas was clean air. However, all the measurements were apparently laminar, because nondimensional heating always decreased with increasing Reynolds number.

Little and Boudreau measured heating and obtained schlieren images for the Viking probe to Mars [97]. The measurements were

made in the conical nozzle of the arc-driven Tunnel F using nitrogen. The flow apparently remained laminar for all tests; the maximum value of Re_D was 0.914×10^6 ([97], Table 2). High-frequency bow shock oscillations were detected in schlieren movies at about 2 kHz, resulting in large scatter in the windward heating measurements. It seems possible that these oscillations may relate to those observed in Fig. 33.

Wright et al. infer transition in the base heating in the Viking flight data at $Re_D \simeq 5 \times 10^6$, based on a change in slope [16]. Edquist et al. performed a modern computation of the Viking Lander 1 using Navier–Stokes methods, encountering various computational difficulties that precluded saying anything definite about transition [98]. This again points out that transition is only one of several major uncertainties in predicting these flows.

Mars Science Laboratory

Lockwood et al. discuss entry issues for the Mars Smart Lander [now the Mars Science Laboratory (MSL)] [99]. MSL is to be a 70-deg sphere-cone forebody with a biconic afterbody [100]. Because MSL has nearly three times the mass of Viking, and a 1/3-larger diameter, transition is much more likely due to the higher Reynolds number, so the aerothermodynamics is not trivial despite the use of a very similar outer mold line [100]. Lockwood's work was focused towards developing a guided reentry, attaining a precise landing point, within less than 10 km, as opposed to the hundreds of kilometers of uncertainty present in previous uncontrolled reentries. It is clear that various new designs could perform much better than the 70-deg half-angle blunt cone that was flight-qualified by Viking et al. It is also clear that the program managers do not want to expend limited resources on the aeroshell, and therefore have insisted on a minimal shift from previously flight-qualified technologies. Horvath et al. [101] present a detailed study of one possible new configuration. A flap was used to provide larger L/D for a greater maneuvering capability while still maintaining an acceptable center of gravity. However, considerable effort would be required to flight-qualify this new configuration.

Edquist and Alter made Navier–Stokes simulations of two MSL configurations that use tabs for trimming [102]. A Baldwin–Lomax model was used for turbulence. Transition was estimated to occur when $Re_\theta \simeq 200$. Although the laminar heating is higher on the windward side of the face, the turbulent heating is higher on the leeward side, which has a longer running length. The heating to the lee side of the face triples at boundary-layer transition, at the peak heating point where the velocity is 4.9 km/s ([102], Fig. 20). The face-averaged peak heating is 1.75 times higher when turbulence occurs; transition is expected before peak heating [17].

Wright et al. performed real-gas Navier–Stokes simulations for comparison to experiments in the T5 hypervelocity shock tunnel [103]. Transition is likely to occur before the peak heating point in the MSL trajectory. Because turbulent peak heating is more than double the laminar peak heating, transition is an important issue. The 7-in.-diam smooth model was placed just downstream of the 12-in.-diam nozzle exit, without blockage difficulties according to the schlieren images (Hans Hornung, private communication, April 2005). The 70-deg sphere cone was tested in pure carbon dioxide. Transition onset on the centerplane occurred for $Re_\theta/M_e \simeq 340$–620, generally decreasing with increasing Re_D and nearly independent of enthalpy. Facility-related effects such as noise remain to be addressed. The authors of [103] believe that transition on the real vehicle will probably be dominated by roughness effects due to ablation.

Hollis et al. [100] report measurements on the Mars Science Laboratory entry vehicle in three tunnels: the 20-in. Mach-6 perfect-gas air tunnel at NASA Langley, the Mach-5 high-enthalpy T5 free-piston shock tunnel at Caltech, and the Mach-7 high-enthalpy LENS shock tunnel at CUBRC. The shock-tunnel measurements were carried out in carbon dioxide to better represent the Martian atmosphere [104]. Computational comparisons were made using the LAURA thin-layer Navier–Stokes code, which can incorporate perfect gas, equilibrium, or nonequilibrium air models. The

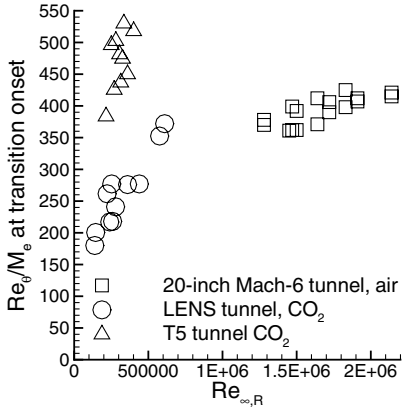

Fig. 42 Transition onset for MSL in three tunnels. Redrawn after Fig. 19 in [100].

Baldwin–Lomax model was used for turbulence. The laminar measurements from the Langley tunnel agreed with laminar perfect-gas solutions to within 5–10% except in the shoulder region. Transition onset was determined by the departure from the laminar solutions. Although many experiments exhibited transition onset, few reached the end of transition. Transition usually occurred first on the lee side of the blunt face. However, heating levels also increased above laminar on the wind side at high Reynolds number, probably due to transition ([100], p. 6). Although higher heating levels on the windward side were unusual in the T5 and Langley measurements, they were common in the LENS tests. Heating increased by a factor of up to 5.5 when transition occurred ([100], Fig. 21).

Hollis et al. tested several transition correlations, including the popular Re_θ/M_e. Their Fig. 19 was redrawn from tabulated data as Fig. 42, which includes only the data where transition occurred on the 70-deg sphere-cone model (the air measurements were also made with other geometries). Figure 42 plots Re_θ/M_e at transition onset on the lee centerplane vs the Reynolds number based on freestream conditions and the maximum radius from the centerline. The value of Re_θ/M_e scatters from about 175 to 530, with the data in each tunnel forming a separate cluster. Because test gas, Mach number, enthalpy, tunnel noise, model size, and roughness vary among the three datasets, the cause of the discrepancy may not be easy to resolve.

MUSES-C Sample Return

Komurasaki and Candler analyze transition on the MUSES-C sample return capsule using a turbulence model approach [105]. Although the Reynolds number based on diameter is of order 10^4, transition might still occur because the very high heating rates produce carbon-phenolic ablation massflows that are several percent of the freestream massflux. Transition was experimentally measured under these conditions by Kaattari [106], and Fig. 11 in [105] shows a good correlation to the experiments when one choice of turbulence model is made. The computed increases in heating rate upon transition are locally of the order of 30%. Park and Balakrishnan also suggested that ablation-induced fluctuations can cause enhanced laminar heating or transition, which was an issue for the Galileo probe [107].

Yamada et al. measured heat-transfer on the MUSES-C shape in a shock tunnel at Mach 10, using an infrared camera. A line of blowing was used to simulate ablation. The heating increased away from the stagnation point for Reynolds numbers of 40,000 and gas injection rates of 2%, which was taken as evidence of transition [108].

Sawada computed heat transfer and ablation on MUSES-C and four Pioneer-Venus probes [109]. Transition is one possible explanation for the higher-than-expected heating rates observed away from the stagnation point for the Galileo and Pioneer probes. Milos analyzed the heat-shield ablation on Galileo, and found higher-than-expected ablation away from the stagnation point, with lower-than-expected ablation near the stagnation point [110]. Sawada uses Park's injection-induced turbulence model to compute

the temperature variations on the Pioneer probe, yielding fairly good agreement, and indicating that transition did occur on one of the four probes. Qualitative agreement with Kaattari's data is also shown [106]. The results suggest that transition may have occurred on several planetary probes, with significant implications for heat shield design.

Park et al. review previous MUSES-C research and provide additional analysis [111]. Transition was thought to be likely downstream of the stagnation point, based on the crude correlations available. The MUSES-C heat shield was thus designed with a uniform thickness, to allow for off-stagnation turbulent heating rates equal to the laminar values at the stagnation point. Again, there are many uncertainties in these complex ablating flows, and the expensive conservatism of existing designs could be reduced through an aerothermodynamics research program that included transition; such a program would also reduce risk.

Express

Suzuki and Abe use correlations and experiments to show that transition is unlikely to affect the aerothermodynamics of the Express capsule [112]. This is because very crude correlations show that transition is likely to be delayed to the supersonic or transonic regime, where aeroheating is not an issue, and experiments show the aerodynamics are not significantly affected. In an earlier paper, the same authors point out that transition in the wake could affect wake closure and the dynamic pressure distribution, which are important for parachute deployment [113].

Titan Probes

Olejniczak et al. performed computations on a 70-deg blunt cone in nitrogen, for application to Titan probes [114]. The measurements were made in the hypervelocity T5 free-piston shock tunnel with a 7-in.-diam model just downstream of the exit of the 12-in.-diam nozzle. Real-gas computations of the nozzle flow past the model were obtained with a Navier–Stokes code. Although laminar runs agreed well with the computations, turbulent heating was augmented above simulated values. An attempt was made to correlate transition with the usual Re_θ or Re_θ/M_e parameters. At zero AOA, transition occurred for $Re_\theta \simeq 130$–170 and $Re_\theta/M_e \simeq 280$–390. Although Re_θ at transition increased with AOA to 260–340 at 25 deg, Re_θ/M_e remained nearly constant at transition as AOA was varied, with values of about 290–390, despite the subsonic value of M_e on the whole face. It remains to be seen whether the correlation can be extended to other wind tunnels or to flight.

Recommendations for Future Work

The design of reentry capsules and planetary probes should take into account the uncertainty in predicting transition and other complex aerothermodynamic phenomena. Preliminary design will have to be carried out using simple correlating parameters, which might include Re_θ/M_e, crossflow Reynolds number, and Re_k. Although none of the many extant methods provide high-accuracy correlations for a wide range of flight data, they remain useful for preliminary design [115,116]. However, the analysis should be carried out for a reasonable range of values, because, for example, Re_θ/M_e scatters between about 50 and 500 in a classic survey of slender ballistic reentry vehicles that transitioned near zero angle of attack [116]. Correlations used for preliminary design should be calibrated against a wide range of data, under conditions as close as possible to those anticipated in flight, using the same analysis methods to be used for the flight predictions, and the scatter in the correlation should be reported, along with information about the calibrating dataset. Several such correlations should be used, for preliminary assessment of different mechanisms, such as roughness and crossflow. Some of the data reviewed here should prove useful for this process, which will provide some assessment of the uncertainty in estimating transition. The effect of this uncertainty should then be evaluated in terms of aerothermodynamic properties such as heat shield weight, to determine if the additional resources required by more advanced estimation methods is justified by the importance to the program. If the uncertainty in estimating transition has a major effect on the program, this should justify the use of advanced computational and experimental methods [117].

The scatter shown in Fig. 42 underscores this need for careful assessment of the simple correlations; it also shows the need for advanced transition models that are based on the physical mechanisms. Transition can be very sensitive to small variations in conditions, in a way which is often not appreciated by the uninitiated. Transition depends on many factors, including Mach number, Reynolds number, wall surface temperature and roughness, freestream noise and chemistry, and so on. Flight conditions will differ from those in *any* tunnel. If transition data are obtained in only one tunnel, a correlation may be developed that seems to be consistent and has little scatter. However, data from one tunnel are therefore often misleading. It is only when transition data are obtained in several facilities under varying conditions that one starts to have any idea of the uncertainties involved in such a correlation. Tunnel-to-tunnel uncertainties give at least *some* measure of the uncertainty in the extrapolation to flight. Mechanism-based transition prediction methods supported by theory, computation, and flight are needed, along with stability and transition data from several tunnels, including quiet tunnels and ballistic ranges, to begin to develop good confidence in extrapolating to new flight conditions.

Summary

Although it appears that viscous effects and transition can affect the vehicle aerodynamics, it also appears that it is relatively simple to adapt the guidance algorithms to make the landing accuracy relatively insensitive to the aerodynamics. The best cases for improved L/D and improved aerothermodynamics may be 1) the increased landing flexibility that can be provided by larger allowable variations in downrange and cross-range, and 2) the larger, more reliable, and thus safer entry window that would be provided by a larger and more reliable L/D.

The two clear transition-related issues appear to be 1) transition on the heat-shield face, and 2) transition and reattachment of the shear layer from the heat-shield rim.

1) Transition appears to have occurred on the heat-shield face during reentry of Apollo, Galileo, and three of the Pioneer-Venus probes, among others. Transition here affects the heat-shield weight, and also the separation from the rim. Because weight is always critical for reentry vehicles, and is particularly critical for those returning from other planets, transition research may be needed.

2) Transition and reattachment in the separated shear layer from the heat-shield rim affects heating and aerodynamic moments. Reattachment was shown to create localized afterbody heating that was 40–75% of stagnation for the Mars Sample Return Orbiter. Similarly high levels of reattachment heating were shown on Mercury and Gemini. Because reattachment heating can be very large, avoiding it becomes a design criterion for the afterbody, and thus an important research area. This same effect may have caused the burn-through on Gemini II, and the high afterbody heating rates on some Apollo flights, although this remains to be determined. In addition, the Mercury and Gemini data show effects of reattachment on trim angle, aerodynamic moments, and aerodynamic stability.

Both of these issues are affected by trajectory and configuration, of course, so their relevance depends on the designs likely to be chosen. However, if transition is at all possible during flight, it should be considered in the initial design stages, so that avoiding transitional heating can be a part of the main design process. This argument may justify transition research for these vehicles, to reduce the risk of failures or late-stage design fixes and the associate cost and weight growth.

Acknowledgments

Tom Horvath and other personnel from the Aerothermodynamics Branch at NASA Langley brought the author's attention to some of the references cited here, and aided in obtaining some of the images

and references. Tom also provided some of the initial motivation. Karl Edquist from Langley provided unpublished data for the Mars Smart Lander. Brian Hollis from Langley provided tabulated data for Fig. 42. Dan Reda from NASA Ames suggested some of the Chul Park references. Mike Wright from NASA Ames provided a prepublication draft of his review article, and several useful comments. Alicia Bagby from NASA Langley was helpful in procuring archival photographs, and Sharon Jiles from NASA STI was also helpful in procuring original paper copies of several archival documents to allow the study of good-quality images. Lynn Albaugh from NASA Ames also provided good-quality images from the Ames photo archive. Stan Bouslog from NASA JSC provided an explanation for the assumptions in [92]. The referees also provided helpful comments.

References

[1] Aldridge, E. C., Jr., Fiorina, C. S., Jackson, M. P., Leshin, L. A., Lyles, L. L., Spudis, P. D., Tyson, N. D., Walker, R. S., and Zuber, M. T., "A Journey to Inspire, Innovate, and Discover," Report of the President's Commission on Implementation of the United States Space Policy, June 2004, www.nasa.gov/pdf/60736main_M2M_report_small.pdf [cited 3 Oct. 2006].

[2] Griffin, M. D., and French, J. R., *Space Vehicle Design*, 2nd ed., AIAA, Reston, VA, 2004.

[3] Anderson, J. D., *Hypersonic and High Temperature Gas Dynamics*, McGraw–Hill, New York, 1989; Reprinted by AIAA, Reston, VA, 2000.

[4] Schneider, S. P., "Hypersonic Laminar-Turbulent Transition on Circular Cones and Scramjet Forebodies," *Progress in Aerospace Sciences*, Vol. 40, Nos. 1–2, 2004, pp. 1–50.

[5] Coleman, W. D., Hearne, L. F., Lefferdo, J. M., and Vojvodich, N. S., "A Study of the Effects of Environmental and Ablator Performance Uncertainties on Heat Shielding Requirements for Blunt and Slender Hyperbolic-Entry Vehicles," AIAA Paper 68-154, Jan. 1968.

[6] Hall, R. D., and Shayler, D. J., *Soyuz: A Universal Spacecraft*, Springer, London, 2003.

[7] Schneider, S. P., "Laminar-Turbulent Transition on Reentry Capsules and Planetary Probes," AIAA Paper 2005-4763, June 2005.

[8] Beckwith, I. E., and Miller, C. G., III, "Aerothermodynamics and Transition in High-Speed Wind Tunnels at NASA Langley," *Annual Review of Fluid Mechanics*, Vol. 22, 1990, pp. 419–439.

[9] Schneider, S. P., "Effects of High-Speed Tunnel Noise on Laminar-Turbulent Transition," *Journal of Spacecraft and Rockets*, Vol. 38, No. 3, May–June 2001, pp. 323–333.

[10] Schneider, S. P., "Flight Data for Boundary-Layer Transition at Hypersonic and Supersonic Speeds," *Journal of Spacecraft and Rockets*, Vol. 36, No. 1, 1999, pp. 8–20.

[11] Reda, D. C., "Review and Synthesis of Roughness-Dominated Transition Correlations for Reentry Applications," *Journal of Spacecraft and Rockets*, Vol. 39, No. 2, March–April 2002, pp. 161–167.

[12] Pate, S. R., "Supersonic Boundary-Layer Transition: Effects of Roughness and Freestream Disturbances," *AIAA Journal*, Vol. 9, No. 5, May 1971, pp. 797–803.

[13] Johnson, H., Candler, G. V., and Wright, M. J., "Boundary Layer Stability Analysis of Mars Science Laboratory Aeroshell," AIAA Paper 2006-0920, Jan. 2006.

[14] Horvath, T. J., Berry, S. A., and Merski, N. R., "Hypersonic Boundary/Shear Layer Transition for Blunt to Slender Configurations—A NASA Langley Experimental Perspective," *Enhancement of NATO Military Flight Vehicle Performance by Management of Interacting Boundary Layer Transition and Separation*, NATO RTO-MP-AVT-111, Oct. 2004; also Paper AVT-111-22, presented at the Applied Vehicle Technology Panel and Specialist's meeting, Prague, Czech Republic.

[15] Wright, M. J., Brown, J. L., Sinha, K., Candler, G. V., Milos, F. S., and Prabhu, D. K., "Validation of Afterbody Aeroheating Predictions for Planetary Probes: Status and Future Work," NASA, Technical Report CP 2004-213456, Aug. 2004, pp. 275–285.

[16] Wright, M. J., Milos, F. S., and Tran, P., "Survey of Afterbody Aeroheating Flight Data for Planetary Probe Thermal Protection System Design," AIAA Paper 2005-4815, June 2005.

[17] Edquist, K. T., Liechty, D. S., Hollis, B. R., Alter, S. J., and Loomis, M. P., "Aeroheating Environments for a Mars Smart Lander," AIAA Paper 2002-4505, Aug. 2002.

[18] Edquist, K. T., Liechty, D. S., Hollis, B. R., Alter, S. J., and Loomis, M. P., "Aeroheating Environments for a Mars Smart Lander," *Journal of Spacecraft and Rockets*, Vol. 43, No. 2, March–April 2006, pp. 330–339.

[19] Horvath, T. J., Heiner, N. C., Olguin, D. M., Cheatwood, F. M., and Gnoffo, P. A., "Afterbody Heating Characteristics of a Proposed Mars Sample Return Orbiter," AIAA Paper 2001-3068, June 2001.

[20] Horvath, T. J., Heiner, N. C., and Olguin, D. M., "Wake Closure and Afterbody Heating on a Mars Sample Return Orbiter," *Journal of Spacecraft and Rockets*, Vol. 41, No. 5, Sept.–Oct. 2004, pp. 705–715.

[21] Smith, A., "Entry and Vehicle Design Considerations," *Capsule Aerothermodynamics*, AGARD R-808, March 1995.

[22] Sinha, K., Barnhardt, M., and Candler, G. V., "Detached Eddy Simulation of Hypersonic Base Flows with Application to Fire II Experiments," AIAA Paper 2004-2633, June 2004.

[23] Sommer, S. C., Short, B. J., and Compton, D. L., "Free-Flight Measurements of Static and Dynamic Stability of Models of the Project Mercury Re-Entry Capsule at Mach Numbers 3 and 9.5," NASA, Technical Memorandum TM-X-373, Aug. 1960.

[24] Taylor, N. L., Hodge, W. F., and Burbank, P. B., "Heat-Transfer and Pressure Measurements of a 1/7-Scale Model of a Mercury Capsule at Angles of Attack from 0 to 20 deg at Mach Numbers of 3.50 and 4.44," NASA, Technical Memorandum TM-X-522, June 1961.

[25] Everhart, P. E., and Bernot, P. T., "Measurements of the Surface Flows, Heat Transfer, Pressure Distribution, and Longitudinal Stability of a Mercury Capsule Model at Mach Numbers of 6.9 and 9.6," NASA, Technical Memorandum TM-X-458, April 1961.

[26] Reller, J. O., Jr., and Seegmiller, H. L., "Pressure and Heat-Transfer Measurements on a Mercury Capsule Model," NASA, Technical Memorandum TM-X-647, May 1962.

[27] Erb, R. B., and Jacobs, S., "Entry Performance of the Mercury Spacecraft Heat Shield," NASA TM-X-57097, STI citation 66N15350, Oct. 1964.

[28] O'Neal, R. L., and Rabb, L., "Heat-Shield Performance During Atmospheric Entry of Project Mercury Research and Development Vehicle," NASA, Technical Memorandum TM-X-490, May 1961.

[29] Stephens, E. W., "Afterbody Heating Data Obtained from an Atlas-Boosted Mercury Configuration in a Free Body Reentry," NASA, Technical Memorandum TM-X-493, Aug. 1961.

[30] Weston, K. C., and Swanson, J. E., "A Compilation of Wind-Tunnel Heat-Transfer Measurements on the Afterbody of the Project Mercury Capsule Reentry Configuration," NASA, Technical Memorandum TM-X-495, Aug. 1961.

[31] Murphy, J. D., "Flight Test Aerodynamic Heating Data for the Afterbody of the Project Mercury Spacecraft with Comparisons to Available Prediction Methods," NASA, Technical Report CR-649, June 1967.

[32] Kruse, R. L., Malcolm, G. N., and Short, B. J., "Comparison of Free-Flight Measurements of Stability of the Gemini and Mercury Capsules at Mach Numbers 3 and 9.5," NASA, Technical Memorandum TM-X-957, April 1964.

[33] Mitchell, W. S., Maynard, O. E., and Arabian, D. D., "Gemini Results as Related to the Apollo Program," *Gemini Summary Conference*, NASA SP-138, Feb. 1967, pp. 329–336.

[34] Box, D. M., Harpold, J. C., Paddock, S. G., Armstrong, N. A., and Hamby, W. H., "Controlled Reentry," *Gemini Summary Conference*, NASA SP-138, Feb. 1967, pp. 159–166.

[35] Griffith, B. J., "Comparison of Aerodynamic Data from the Gemini Flights and AEDC-VKF Wind Tunnels," *Journal of Spacecraft and Rockets*, Vol. 4, No. 7, July 1967, pp. 919–924.

[36] Pershing, B. M., "The Hypersonic Aerodynamic Characteristics of the Gemini Re-Entry Module Based on a Statistical Analysis of Wind Tunnel Test Data," Aerospace Corporation, Aerospace Report TOR-0150(3107-15)-8, June 1968, DTIC citation AD856691.

[37] Bertin, J. J., and Cummings, R. M., "Fifty Years of Hypersonics: Where We've Been, Where We're Going," *Progress in Aerospace Sciences*, Vol. 39, Nos. 6–7, Aug.–Oct. 2003, pp. 511–536.

[38] Malik, P. W., and Souris, G. A., "Project Gemini: A Technical Summary," NASA, Contractor Report CR-1106, June 1968.

[39] Collins, D. R., Dotts, H. W., Hoyler, W. F., and Hecht, K. F., "Spacecraft Development," *Gemini Midprogram Conference, Including Experiment Results*, NASA SP-121, Feb. 1966, pp. 15–23.

[40] Gemini Program, "Gemini Program Mission Report GT-2, Gemini 2," NASA, Technical Memorandum NASA-TM-X-57103, Feb. 1965, NASA citation 75N75478.

[41] Sheldon, G. J., "Re-Entry Module/Adaptor Interconnect Fairing Aerodynamic Heating Wind Tunnel Tests AEDC Tunnel B," McDonnell Company, Final report, Dec. 1967, DTIC citation AD-856658.

[42] Anon., "Gemini-B Re-Entry Module/Adaptor Attachment Fairing Aerodynamic Heating and Pressure Tests in the McDonnell

Hypervelocity Impulse Tunnel–Series 1," McDonnell Company, Technical Report MAC-G004-Vol-1, Dec. 1967, DTIC citation AD-856900.
[43] Anon., "Gemini-B Re-Entry Module/Adaptor Attachment Fairing Aerodynamic Heating and Pressure Tests in the McDonnell Hypervelocity Impulse Tunnel–Series 1," McDonnell Company, Technical Report MAC-G004-Vol-2, Dec. 1967, DTIC citation AD-856901.
[44] Raper, R. M., "Heat-Transfer and Pressure Measurements Obtained During Launch and Reentry of the First Four Gemini-Titan Missions and Some Comparisons with Wind-Tunnel Data," NASA Technical Memorandum TM-X-1407, Aug. 1967.
[45] Pritts, O. R., and Merz, G. H., "Pressure and Heat-Transfer Distributions on Exit and Re-Entry Configurations of the Gemini Spacecraft at Mach Number 8 and 10," AEDC Technical Report AEDC-TDR-63-100, July 1963.
[46] Price, E. A., Jr., Stallings, R. L., Jr., and Howard, P. W., "Pressure and Heat-Transfer Distributions of 0.1-Scale Gemini Exit and Reentry Models at Mach Numbers of 3.51 and 4.44," NASA Technical Memorandum TM-X-1149, Sept. 1965.
[47] Kruse, R. L., "Transition and Flow Reattachment Behind an Apollo-Like Body at Mach Numbers to 9," NASA Technical Note TN-D-4645, July 1968.
[48] Wright, M. J., Prabhu, D. K., and Martinez, E. R., "Analysis of Afterbody Heating Rates on the Apollo Command Modules, Part 1: AS-202," AIAA Paper 2004-2456, June 2004.
[49] Canning, T. N., and Sommer, S. C., "Investigation of Boundary-Layer Transition on Flat-Faced Bodies of Revolution at High Supersonic Speeds," NACA Research Memorandum RM-A57C25, June 1957, NASA STI citation 93R18985.
[50] Walters, E. W., "Free-Flight Measurements of Radiative Heating to the Front Face of the Apollo Reentry Capsule as a Function of Angle of Attack," NASA, Technical Memorandum NASA-TM-X-851, Feb. 1964.
[51] Chapman, G. T., and Jackson, C. T., Jr., "A Free-Flight Investigation of the Heat Transfer and Afterbody Flow Field of an Apollo-Type Configuration at Speeds to 10,000 ft/sec," NASA Technical Memorandum NASA-TM-X-853, Nov. 1963.
[52] Crowder, R. S., and Moote, J. D., "Apollo Entry Aerodynamics," AIAA Paper 68-1008, Oct. 1968.
[53] Graves, C. A., and Harpold, J. C., "Re-Entry Targeting Philosophy and Flight Results from Apollo 10 and 11," AIAA Paper 70-28, Jan. 1970.
[54] Low, G., "Apollo 11 Mission Report," NASA Technical Report MSC-00171, 1969, NASA citation 70N17401.
[55] Honegger, B., and Brandli, H., "Saving Apollo 11," *Aviation Week and Space Technology*, Dec. 2004, pp. 79–80.
[56] Hillje, E. R., "Entry Flight Aerodynamics from Apollo Mission AS-202," NASA Technical Note NASA-TN-D-4185, Oct. 1967.
[57] Hillje, E. R., "Entry Aerodynamics at Lunar Return Conditions Obtained from the Flight of Apollo 4 (AS-501)," NASA Technical Note NASA-TN-D-5399, Oct. 1969.
[58] Griffith, B. J., and Boylan, D. E., "Postflight Apollo Command Module Aerodynamic Simulation Tests," *Journal of Spacecraft and Rockets*, Vol. 5, No. 7, July 1968, pp. 843–848.
[59] Griffith, B. J., and Boylan, D. E., "Reynolds and Mach Number Simulation of Apollo and Gemini Re-Entry and Comparison with Flight," *Hypersonic Boundary Layers and Flow Fields*, AGARD CP-30, Paper 8.
[60] Hillje, E. R., and Savage, R.. "Status of Aerodynamic Characteristics of the Apollo Entry Configuration," AIAA Paper 68-1143, Dec. 1968.
[61] Graves, C. A., and Harpold, J. C., "Apollo Experience Report—Mission Planning for Apollo Entry," NASA Technical Note NASA-TN-D-6725, March 1972.
[62] Harpold, J. C., "Minimum Lift-to-Drag Ratio Requirement for the Lunar Mission," NASA Technical Memorandum NASA-TM-X-69752, Oct. 1967, NASA STI citation 74N70848.
[63] Berry, S. A., Horvath, T. J., Weilmuenster, K. J., Alter, S. J., and Merski, N. R., "X-38 Experimental Aeroheating at Mach 10," AIAA Paper 2001-2828, June 2001.
[64] Bell Comm. Co., "Some Effects on the Apollo Mission of Reducing the Maximum Reentry Range," NASA Contractor Report NASA-CR-111052, June 1964, NASA citation 79N71907.
[65] Pavlosky, J. E., and St. Leger, L. G., "Apollo Experience Report—Thermal Protection Subsystem," NASA Technical Note NASA-TN-D-7564, Jan. 1974.
[66] Erb, R. B., Greenshields, D. H., Chauvin, L. T., Pavlosky, J. E., and Statham, C. L., "Apollo Thermal-Protection System Development," *Journal of Spacecraft and Rockets*, Vol. 7, No. 6, June 1970, pp. 727–734.
[67] Erb, R. B., Greenshields, D. H., Chauvin, L. T., Pavlosky, J. E., and Statham, C. L., "Apollo Thermal-Protection System Development," AIAA Paper 68-1142, Dec. 1968.
[68] Anon. (North American Aviation Staff), "Design Criteria, Trajectories, and Heating Rates for the Apollo Command Module Heat Shield, Volume 1," NASA Technical Report CR-117561, June 1963; NASA STI citation 79N76584.
[69] Lee, D. B., "Trajectory Influence on the Heating Distribution Around the Apollo Command Module," NASA Technical Memorandum NASA-TM-X-65127, May 1965.
[70] Bertin, J. J., "Wind-Tunnel Heating Rates for the Apollo Spacecraft," NASA Technical Memorandum NASA-TM-X-1033, Jan. 1965 (limited distribution).
[71] Weston, K. C., and Fitzkee, A. L., "Afterbody Heat Transfer Measurements Obtained During Reentry of the Spacecraft of the Mercury-Atlas 5 Mission," NASA Technical Memorandum NASA-TM-X-564, Dec. 1963 (limited distribution).
[72] Jones, R. A., "Wind-Tunnel Measurements of Transition on the Face of a Blunt Entry Capsule at Angle of Attack," *AIAA Journal*, Vol. 6, No. 3, March 1968, pp. 545–546.
[73] Jones, R. A., "Measured Heat-Transfer and Pressure Distributions on the Apollo Face at a Mach Number of 8 and Estimates for Flight Conditions," NASA Technical Memorandum NASA-TM-X-919, April 1964.
[74] Jones, R. A., "Preliminary Results on Heat-Transfer to the Afterbody of the Apollo Reentry Configuration at a Mach Number of 8," NASA Technical Memorandum NASA-TM-X-699, Sept. 1962; Superseded by NASA TM-X-813.
[75] Jones, R. A., "Experimental Investigation of the Overall Pressure Distribution, Flow Field, and Afterbody Heat-Transfer Distribution of an Apollo Reentry Configuration at a Mach Number of 8," NASA Technical Memorandum NASA-TM-X-813, June 1963; Supersedes NASA TM-X-699.
[76] Jones, J. J., and Moore, J. A., "Shock-Tunnel Heat Transfer Investigation on the Afterbody of an Apollo-Type Configuration at Angles of Attack up to 45 deg," NASA Technical Memorandum NASA-TM-X-1042, Dec. 1965.
[77] Marvin, J. G., Tendeland, T., and Kussoy, M., "Apollo Forebody Pressure and Heat-Transfer Distributions in Helium at Mach 20," NASA Technical Memorandum NASA-TM-X-854, Nov. 1963.
[78] Lees, L., "Laminar Heat Transfer over Blunt-Nosed Bodies at Hypersonic Flight Speeds," *Jet Propulsion*, Vol. 26, April 1956, pp. 259–269.
[79] Marvin, J. G., and Kussoy, M., "Experimental Investigation of the Flow Field and Heat-Transfer over the Apollo-Capsule Afterbody at a Mach Number of 20," NASA Technical Memorandum NASA-TM-X-1032, Feb. 1965.
[80] Lee, G., "Correlation of Heat-Transfer Data for the Apollo Afterbody at Mach Numbers 8 to 20," NASA Technical Memorandum NASA-TM-X-855, Feb. 1964.
[81] Bertin, J. J., Lee, D. E., and Ried, R. C., "Apollo Reentry Heating," NASA Technical Memorandum NASA-TM-X-66780, Sept. 1963, NASA STI citation 79N76503.
[82] Smith, A. M. O., and Clutter, D. W., "The Smallest Height of Roughness Capable of Affecting Boundary-Layer Transition," *Journal of the Aerospace Sciences*, Vol. 26, No. 4, April 1959, pp. 229–245.
[83] Bertin, J. J., "The Effect of Protuberances, Cavities, and Angle of Attack on the Wind-Tunnel Pressure and Heat-Transfer Distribution for the Apollo Command Module," NASA Technical Memorandum NASA-TM-X-1243, Oct. 1966.
[84] Mosely, W. C., Jr., and Martino, J. C., "Apollo Wind Tunnel Testing Program—Historical Development of General Configurations," NASA Technical Note NASA-TN-D-3748, Dec. 1966.
[85] Yee, L., "Free-Flight Measurements of Heat Transferred to the Apollo Afterbody with and Without Heat Shield Ablation," NASA Technical Memorandum NASA-TM-X-1096, April 1965.
[86] Lee, D. B., "Apollo Experience Report—Aerothermodynamics Evaluation," NASA Technical Note NASA-TN-D-6843, June 1972.
[87] Lee, D. B., Bertin, J. J., and Goodrich, W. D., "Heat-Transfer Rate and Pressure Measurements Obtained During Apollo Orbital Entries," NASA Technical Note NASA-TN-D-6028, Oct. 1970.
[88] Lee, D. B., and Goodrich, W. D., "The Aerothermodynamic Environment of the Apollo Command Module During Superorbital Entry," NASA Technical Note NASA-TN-D-6792, April 1972.
[89] Bartlett, E. P., Nicolet, W. E., Abbett, M. J., and Moyer, C. B., "Improved Heat-Shield Design Procedures for Manned Entry Systems. Part 2: Application to Apollo; Final Report," NASA

Contractor Report NASA-CR-108689, June 1970, NASA citation 94N71373.
[90] Bartlett, E. P., "Improved Heat-Shield Design Procedures for Manned Entry systems. Part 1: Executive Summary; Final Report," NASA Contractor Report NASA-CR-108688, June 1970, NASA citation 94N71374.
[91] Bartlett, E. P., and Curry, D. M., "An Evaluation of Flight Data for the Apollo Thermal Protection System," *Space Simulation*, NASA SP-298, May 1972, pp. 749–768.
[92] Williams, S. D., Curry, D. M., Bouslog, S. A., and Rochelle, W. C., "Thermal Protection System Design Studies for Lunar Crew Module," *Journal of Spacecraft and Rockets*, Vol. 32, No. 3, May–June 1995, pp. 456–462.
[93] Park, C., and Tauber, M. E., "Heatshielding Problems of Planetary Entry, a Review," AIAA Paper 99-3415, June 1999.
[94] Milos, F. S., "Galileo Probe Heat Shield Ablation Experiment," *Journal of Spacecraft and Rockets*, Vol. 34, No. 6, Nov.–Dec. 1997, pp. 705–713.
[95] Milos, F. S., Chen, Y.-K., Squire, T. H., and Brewer, R. A., "Analyis of Galileo Probe Heatshield Ablation and Temperature Data," *Journal of Spacecraft and Rockets*, Vol. 36, No. 3, May–June 1999, pp. 298–306.
[96] Zappa, O. L., and Reinecke, W. G., "An Experimental Investigation of Base Heating on Typical Mars Entry Body Shapes," NASA Technical Report NASA-CR-1920, Nov. 1971.
[97] Little, H. R., and Boudreau, A. H., "Heat-Transfer Tests on a 14-Percent Scale Model of the NASA-MMC Viking Mars Entry Vehicle at Mach Number 16," AEDC, Technical Report AEDC-TR-73-195, Dec. 1973.
[98] Edquist, K. T., Wright, M. J., and Allen, G. A., Jr., "Viking Afterbody Heating Computations and Comparisons to Flight Data," AIAA Paper 2006-0386, Jan. 2006.
[99] Lockwood, M. K., Sutton, K., Prabhu, R., Powell, R. W., Graves, C. A., Epp, C., and Carman, G. L., "Entry Configurations and Performance Comparisons for the Mars Smart Lander," AIAA Paper 2002-4407, Aug. 2002.
[100] Hollis, B. R., Liechty, D. S., Wright, M. J., Holden, M. S., Wadhams, T. P., MacLean, M., and Dyakonov, A., "Transition Onset and Turbulent Heating Measurements for the Mars Science Laboratory Entry Vehicle," AIAA Paper 2005-1437, Jan. 2005.
[101] Horvath, T. J., O'Connell, T. F., Cheatwood, F. M., Alter, S. J., and Prabhu, R. K., "Experimental Hypersonic Aerodynamic Characteristics of the 2001 Mars Surveyor Precision Lander with Flap," AIAA Paper 2002-4408, Aug. 2002.
[102] Edquist, K. T., and Alter, S. J., "Computational Aeroheating Predictions for Mars Lander Configurations," AIAA Paper 2003-3639, June 2003.
[103] Wright, M. J., Olejniczak, J., Brown, J. L., Hornung, H. G., and Edquist, K. T., "Computational Modeling of T5 Laminar and Turbulent Heating Data on Blunt Cones, Part 2: Mars Applications," AIAA Paper 2005-0177, Jan. 2005.
[104] MacLean, M., Wadhams, T., Holden, M., and Hollis, B. R., "Investigation of Blunt Bodies with CO_2 Test Gas Including Catalytic Effects," AIAA Paper 2005-4693, June 2005.
[105] Komurasaki, K., and Candler, G. V., "Theoretical Consideration on Laminar-to-Turbulent Transitions over an Ablating Reentry Capsule," Japanese Institute of Space and Astronautical Science, Technical Report SP-17, March 2003, NASA citation 20040003940
[106] Kaattari, G. E., "Effects of Mass Addition on Blunt-Body Boundary-Layer Transition and Heat Transfer," NASA Technical Report NASA-TP-1139, Jan. 1978.
[107] Park, C., and Balakrishnan, A., "Ablation of Galileo Probe Heat-Shield Models in a Ballistic Range," *AIAA Journal*, Vol. 23, No. 2, Feb. 1985, pp. 301–308.
[108] Yamada, T., Ogawa, H., Nonaka, S., Inatani, Y., Nakakita, K., and Yamazaki, T., "An Experimental Study on the Boundary Layer Transition Due to Gas Injection from Capsule-Shape Body Surface," Japanese Institute of Space and Astronautical Science, Technical Report SP-17, March 2003, NASA citation 20040003942.
[109] Sawada, K., "Anomalous Heating Profile over Entry Capsule with Ablation and its Relation to Earlier Turbulent Transition," Japanese Institute of Space and Astronautical Science, Technical Report SP-17, March 2003, NASA citation 20040003941.
[110] Milos, F. S., "Galileo Probe Heat Shield Ablation Experiment," AIAA Paper 96-1823, June 1996.
[111] Park, C., Abe, T., and Inatani, Y., "Research on the Heatshield for MUSES-C Earth Reentry," AIAA Paper 98-2852, June 1998.
[112] Suzuki, K., and Abe, T., "Experimental Studies on Boundary-Layer Transition on a Reentry Vehicle at Transonic and Supersonic Speeds," Japanese Institute of Space and Astronautical Science, Technical Report 659, March 1995, NASA citation 95N29712.
[113] Suzuki, K., and Abe, T., "Wind Tunnel Experiments on Wake Flow Field Behind a Reentry Capsule from a Viewpoint of Parachute Deployment at Supersonic Speeds," Japanese Institute of Space and Astronautical Science, Technical Report 655, Dec. 1994, NASA citation 95N26740.
[114] Olejniczak, J., Wright, M. J., Laurence, S., and Hornung, H. G., "Computational Modeling of T5 Laminar and Turbulent Heating Data on Blunt Cones, Part 1: Titan Applications," AIAA Paper 2005-0176, Jan. 2005.
[115] Beckwith, I. E., and Bertram, M. H., "A Survey of NASA Langley Studies on High-Speed Transition and the Quiet Tunnel," NASA, Technical Report TM-X-2566, July 1972, NASA Recon citation 72N26239.
[116] Berkowitz, A. M., Kyriss, C. L., and Martellucci, A., "Boundary Layer Transition Flight Test Observations," AIAA Paper 77-125, Jan. 1977.
[117] Reshotko, E., "Transition Issues at Hypersonic Speeds," AIAA Paper 2006-0707, Jan. 2006.

T. Lin
Associate Editor